Aerodynamic Equilibrium and Stability in Ventilation and Air Quality Control of Complex Urban Tunnels

or

Aerodynamic Equilibrium and Stability for Air Quality Management in Complex Urban Tunnels

Center for Transportation, Environment, and Community Health
Final Report

by

Zhen Tan and H. Oliver Gao
School of Civil and Environmental Engineering, Cornell University, Ithaca, NY 14850, USA

March 10, 2019

DISCLAIMER

The contents of this report reflect the views of the authors, who are responsible for the facts and the accuracy of the information presented herein. This document is disseminated in the interest of information exchange. The report is funded, partially or entirely, by a grant from the U.S. Department of Transportation's University Transportation Centers Program. However, the U.S. Government assumes no liability for the contents or use thereof.

TECHNICAL REPORT STANDARD TITLE PAGE

1. Report No.	2.Government Accession No.	3. Recipient's Catalog No.
4. Title and Subtitle Aerodynamic Equilibrium and Stability in Ventilation and Air Quality Control of Complex Urban Tunnels		5. Report Date March 10, 2019 6. Performing Organization Code
7. Author(s) Zhen Tan and H. Oliver Gao (ORCID #: 0000-0002-7861-9634)		8. Performing Organization Report No.
9. Performing Organization Name and Address School of Civil and Environmental Engineering, Cornell University, Ithaca, NY 14850, USA		10. Work Unit No. 11. Contract or Grant No. 69A3551747119
12. Sponsoring Agency Name and Address U.S. Department of Transportation 1200 New Jersey Avenue, SE Washington, DC 20590		13. Type of Report and Period Covered Final Report Start date: 11/01/2017 End date: 12/31/2018 14. Sponsoring Agency Code US-DOT
15. Supplementary Notes		

16. Abstract

Modern urban vehicular tunnels generally have a branched structure and complex nonlinear aerodynamics. We established and analyzed the 1-D aerodynamic equations and pollutant dispersion model in such bifurcate hydraulic networks. To design a tractable model that captures system complexity, we proposed a novel piecewise-affine (PWA) approximation for the flow-dependent local pressure-loss coefficients at tunnel junctions. This enables us to model the flow system via first-order ordinary differential equations (ODEs) with piecewise-quadratic polynomials. We proved a fundamental and easily verifiable sufficient condition for the uniqueness and stability of the steady-state solution of each ODE piece. We also demonstrated via a numerical study that for the entire system (across different ODE pieces) there may exist multiple stable steady-state solutions, which can lead to different CO concentration distributions in the system. Our study provides a systematic modeling tool and a theoretical foundation for air quality management in complex tunnels.

17. Key Words	18. Distribution Statement
complex urban tunnels, air quality management, ventilation, nonlinear system, stability	A modified version is published in 2018 Annual American Control Conference (ACC) June 27–29, 2018. Wisconsin Center, Milwaukee, USA

19. Security Classif (of this report)	20. Security Classif. (of this page)	21. No of Pages	22. Price
Unclassified	Unclassified		

Form DOT F 1700.7 (8-69)

Aerodynamic Equilibrium and Stability for Air Quality Management in Complex Urban Tunnels

Zhen Tan and H. Oliver Gao

School of Civil and Environmental Engineering, Cornell University, Ithaca, NY 14850, USA

ABSTRACT

Modern urban vehicular tunnels generally have a branched structure and complex nonlinear aerodynamics. We established and analyzed the 1-D aerodynamic equations and pollutant dispersion model in such bifurcate hydraulic networks. To design a tractable model that captures system complexity, we proposed a novel piecewise-affine (PWA) approximation for the flow-dependent local pressure-loss coefficients at tunnel junctions. This enables us to model the flow system via first-order ordinary differential equations (ODEs) with piecewise-quadratic polynomials. We proved a fundamental and easily verifiable sufficient condition for the uniqueness and stability of the steady-state solution of each ODE piece. We also demonstrated via a numerical study that for the entire system (across different ODE pieces) there may exist multiple stable steady-state solutions, which can lead to different CO concentration distributions in the system. Our study provides a systematic modeling tool and a theoretical foundation for air quality management in complex tunnels.

Key words: complex urban tunnels, air quality management, ventilation, nonlinear system, stability

I. Introduction

Underground tunnel transport is a popular solution to traffic congestion in the case of growing population and demand for mobility in a dense urban area. Virtually every major metropolis is constructing or extending its underground transport systems [1], such as the double-decker tunnels on route A86 in Paris and the large-diameter tunnels for route M30 in Madrid [2]. By moving some of the traffic underground, these tunnel facilities also help to improve ambient air quality, because unlike surface traffic emissions, emissions underground are not directly discharged to the open air. However, the high volume of traffic and the quasi-closed nature of the space involved make these tunnels new hotspots for air quality management and control [3], both inside the tunnel and near tunnel portals and vents.

For mitigation of problems that may arise, tunnel ventilation systems are needed to help dilute the pollutant concentration inside the tunnel and discharge the emissions through tunnel portals and vents [4]. Various functional and topographic requirements typically demand that urban tunnels have a mainline-branch structure. The tunnel branches are connected to other underground facilities such as commercial building garages [5] or to the ground network via ramps [6]. The interaction of the airflows in different tunnel branches can lead to complicated aerodynamics, which governs dispersion and transport of air pollutants both inside the tunnel and near the tunnel portals [5]–[8]. Thus quantitative aerodynamic analysis of the complex tunnel system is needed for effective ventilation design and air quality management. For such pipe-junction systems, experimental and computational fluid dynamics (CFD) analyses are usually time-consuming, with considerable work for tasks such as meshing of the junctions [9]. An analytical system model with good accuracy and a compact structure that enables efficient analysis is therefore highly desirable, which is a key purpose of this study.

Longitudinal venting that uses jet fans is the most popular tunnel ventilation scheme, because of its efficiency and relatively low cost [10]. Many studies have been done on aerodynamic modeling of longitudinal ventilation in a simple tunnel, that is, a tunnel without branches (e.g., [11], [12]). In practice, the control of such ventilation systems is based primarily on steady-state flow (a.k.a. equilibrium flow) models [13], [14], hence understanding of the steady-state flow and its stability is crucial to ventilation system design. Because the kinetic equation for air movement in a simple tunnel is univariate (e.g., with a single air-velocity variable), it is straightforward to see that its steady-state flow is unique and stable. The relevant studies that are based on steady-state modeling have proposed static optimal ventilation design and control algorithms for urban loop-branched tunnels [13], [14] or mainline-branch structured bifurcate tunnels [8]. The transient airflow behavior in such systems has also been studied by way of field experiments (e.g. [15]), a scaled model and numerical analysis (e.g., [16]), and analytical modeling (e.g., [17]). In particular, in [17] the airflow rebalancing process inside a simple tunnel after a change in the fan intensity occurs is quantitatively characterized. The results show that the flow can always rebalance and reach a new stable equilibrium.

Extension of such analytical models to bifurcate tunnels is a recent development (e.g., [4], [8]). In particular, in [4] the steady-state and transient flows under fan perturbation were studied, but lacking a rigorous investigation of the system properties. Actually, some recent studies based mainly on system reliability analysis have looked at flow stability in complex mining-tunnel networks (e.g., [18], [19]), but the corresponding issue in complex vehicular tunnels has not been systematically addressed. A more rigorous investigation is needed for the analysis of branched tunnels. One source of complexity in such branched systems is the flow-dependent local pressure loss in the airflow across the branching junctions. In general, the local pressure-loss coefficient for a branched tunnel is not easy to obtain [5], [7], as it depends not only on the tunnel's geometric parameters but also on the relative relations among the mainline flows upstream/downstream of the junction and the flow in the

bilateral branch [9], [20]. In existing studies of urban bifurcate tunnels [4], [8], [21], the local pressure-loss coefficients at branching points were assumed constant. This is because the focus of those studies was a ventilation-control algorithm that could deal with modeling errors by use of a feedback structure and estimation techniques [14]. The range of the flow variables in the tunnel that was studied is relatively narrow, hence the local loss coefficients vary only slightly and the geometry is simple (e.g., with only a small lateral branch angle). In this study we aim to establish an analytical framework for analyzing general bifurcate tunnels, so possible variations in the flow-dependent local pressure-loss coefficients are explicitly modeled.

Significant work has been done in empirical formulae (e.g., [22]) and analytical formulae (e.g., [9], [23]) for computing such coefficients in branched-pipe systems. One of the most popular and convenient analytical models was proposed in [9] for all kinds of "T-junctions" with either "separating flow" or "joining flow," which cover all possible cases of branching in bifurcate tunnels. The results were derived from the 1-D momentum equation for incompressible flow, and comprehensive experiments verified the accuracy of this model [9]. Since the air velocity inside a tunnel is normally less than 10 m/s [20], the Mach number of the flow is less than 0.2, hence models based on incompressible flow can be applied to compute the local pressure-loss coefficients in tunnel systems [9]. However, such models are still quite complicated, as they represent the pressure-loss coefficients as nonlinear functions of the flow-ratio variables (e.g., the formulae in [9]). To make the analysis easier hence more practical, we propose a piecewise-affine (PWA) approximation for these complicated functions in a specially designed one-to-one transformation of the original flow-ratio variables. This enables us to formulate the problem of the steady-state flow by solving a number of systems of quadratic equations for their respective convex feasible regions. Further, we show that under an easily checkable sufficient condition, each system of quadratic equations has at most one steady-state solution, which admits the use of efficient algorithms to find the solution (e.g., [24]). In addition, we prove that the same condition is sufficient for system stability.

In the next section, we present the modeling setup and basic aerodynamic equations and pollutant dispersion model. Section III introduces the PWA model for the local pressure loss coefficients; Section IV integrates the models in Section II and III and discusses the properties of the steady-state flow solutions. A numerical example is provided in Section V, and we conclude in the last section.

II. Aerodynamic and Pollutant Dispersion Modelling of Bifurcate Tunnels

A. System decomposition

The airflow inside a tunnel is driven mainly by jet fans, while moving vehicles also impose a force on the airflow. If the direction of the traffic is consistent with that of the ventilation and the speed of the traffic is higher than that of the airflow, then the moving vehicles also help to drive the airflow along the direction of the ventilation; otherwise, they cause a force of resistance [7], [20]. Within the airflow field, vehicular emissions are dispersed, transported, and distributed in the system; eventually discharged through tunnel vents and exit portals. Both the transient and steady-state pollutant concentrations inside the tunnel are governed by the behavior of the airflow in the system [15], [17]. It is thus fundamental to understand the flow field in complex tunnels.

As a routine step in tunnel analysis (e.g., [13], [20]), we divide the tunnel into connected control *segments* by the access points of the lateral ramp branches, the upper vents, and any points with changes in alignment or cross section. Then the bifurcate tunnel system can be modeled as an aerodynamic system that has a serial-branch structure. The tunnel segments are indexed by $i \in I = \{1, 2, \ldots, n + m\}$, where $i = 1, \ldots, n$ correspond to the mainline segments ordered in the direction of the longitudinal ventilation, and $i = n + 1, \ldots, n + m$ correspond to the segments of the ramp branches. We order ramps from 1 to m in the direction of the mainline ventilation direction. Without loss of generality, we assume that only the long mainline tunnel has upper vents or variations in the geometric parameters, so each ramp branch is treated as a single segment. Fig.1 shows an example of segmental decomposition of a bifurcate tunnel. We denote by h_i the index of the mainline segment such that the access point of segment $n + i$ (i.e., ramp i), $i \in \{1, \ldots, m\}$ is the division point between the mainline segments h_i and $h_i + 1$. For example, in Fig.1, we have $h_1 = 1$, $h_2 = 2$, $h_{m-1} = n - 3$ and $h_m = n - 2$. For ease of derivation, we also define $h_0 = 1$ and $h_{m+1} = n$. We let I_{in} be the set of indices of ramps in which the air flows into the mainline, and I_{out} as the set of indices of ramps in which the air flows out from the mainline. We also define two index sets, $I_{\text{in}}^{\text{main}} = \{h_j: j = 1, \ldots, m, j \in I_{\text{in}}\}$ and $I_{\text{out}}^{\text{main}} = \{h_j + 1: j = 1, \ldots, m, j \in I_{\text{out}}\}$, to denote the mainline segments that are upstream of an inflow junction and downstream of an outflow junction, respectively.

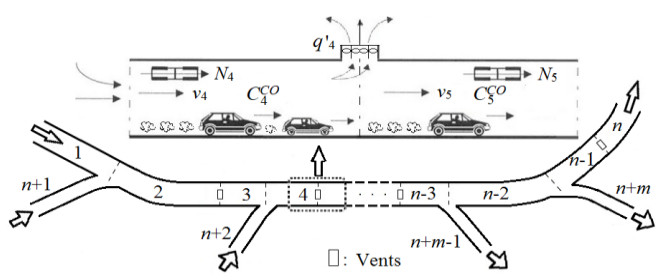

Fig. 1. Complex urban tunnel system

B. Basic and non-basic air-velocity variables

Let $v_i \geq 0$ ($i \in I$) denote the air velocity (averaged over the cross section) in segment i along the predefined required ventilation direction. To facilitate the modeling process, we define a segment index set I_B as the subset of I such that the air velocities in those tunnel segments, $\{v_i, i \in I_B\}$, are independent, and an index set I_N as $I \backslash I_B$; the air velocity v_i in every tunnel segment which is indexed by some i in I_N is a linear combination of the air velocities in I_B plus some constant. We call the variables in $\{v_i, i \in I_B\}$ the *basic* velocity variables, and define $\boldsymbol{v}_B$ as the vector with

components $\{v_i\ ,\ i \in I_B\}$. Since the airflow is regarded as incompressible under low Mach number, we have the following characterization of I_B, which is based on flow conservation.

Lemma 1: For every $i \in \{1,\ldots, m\}$, the index set I_B contains exactly one element from each of two of the three sets $\{n + i\}$, $\{h_{i-1} + 1, h_{i-1} + 2, \ldots, h_i\}$, and $\{h_i, h_i + 1, \ldots, h_{i+1}\}$ (and no element from the third set).

Proof: By the indexing of the tunnel segments and flow conservation (since the airflow is incompressible under low Mach number), the following holds true at every time t:

$$\begin{cases} q_{h_i} = q_{h_i+1} - q_i\,, & \forall n+i \in I_{\text{in}}; \\ q_{h_i} = q_{h_i+1} + q_i\,, & \forall n+i \in I_{\text{out}}; \\ q_{i+1} = q_i + q'_i\,, & \forall i \in \{1,\ldots, n\}, \end{cases} \tag{1}$$

where $q_i = v_iA_i$ is the airflow rate in tunnel segment i (m^3/s), A_i is the cross-sectional area of tunnel segment i (m^2), and q'_i is the air inflow rate from the upper vent at the end of segment i (m^3/s); $q'_i = 0$ if there is no vent at this location.

Since the airflow rate q_i is the air velocity v_i scaled by A_i, the definition of I_B in terms of the air-velocity variables v_i is equivalent to the definition of I_B in terms of the flow-rate variables q_i. For every segment $i \in \{1, \ldots, m\}$, consider the three segment groups $\{n + i\}$, $\{h_{i-1} + 1, h_{i-1} + 2, \ldots, h_i\}$, and $\{h_i, h_i + 1, \ldots, h_{i+1}\}$. Clearly, the linear equations in (1) imply that knowing the value of exactly one flow-rate variable q in each of any two of these three groups is necessary and sufficient to determine the values of all the flow-rate variables q in all three groups. Since the union of these three groups over all i in $\{1, \ldots, m\}$ is I and the third group for ramp i is equal to the second group for ramp $i + 1$ ($i = 1, \ldots, m - 1$), the result follows. ■

Let $\boldsymbol{q}$ be the vector with components $q_1, \ldots, q_{m+n}$. Then we can write the system of linear equations (1) in matrix form, $\boldsymbol{Aq} = \boldsymbol{b}$, where $\boldsymbol{A} \in \mathbb{R}^{(n-1)\times(n+m)}$ is a matrix with full row rank and $\boldsymbol{b} \in \mathbb{R}^{(n+m)}$ is a vector. We reorganize the columns of $\boldsymbol{A}$ as $\boldsymbol{A} = [\boldsymbol{A}_B, \boldsymbol{A}_N]$ in such a way that $\boldsymbol{A}_N$ has full column rank, and we partition the vector $\boldsymbol{q}$ accordingly, as $\boldsymbol{q} = [\boldsymbol{q}_B{}^T, \boldsymbol{q}_N{}^T]^T$. Thus I_B consists of all the column indices of $\boldsymbol{A}_N$ that satisfy this partition.

A standard approach for finding I_B is by QR factorization in order to find $n - 1$ linearly independent columns in $\boldsymbol{A}$. Then I_B consists of the indices of the rest of the columns in $\boldsymbol{A}$. In this application, however, Lemma 1 gives a much easier approach. For example, in this paper we choose I_B to be $\{1, n + 1, n + 2, \ldots, n + m\}$, that is, the tunnel segments that correspond to the mainline entrance and all the ramps. Clearly, $|I_B| = m + 1$, and so the *non-basic* index set $I_N = I \backslash I_B$ has $|I_N| = n - 1$, and by our choice of I_B, $I_N = \{2, 3, \ldots, n\}$.

Since $\boldsymbol{Aq} = \boldsymbol{A}_B\boldsymbol{q}_B + \boldsymbol{A}_N\boldsymbol{q}_N = \boldsymbol{b}$, we have $\boldsymbol{q}_N = \boldsymbol{A}_N{}^{-1}(\boldsymbol{b} - \boldsymbol{A}_B\boldsymbol{q}_B)$. We partition $\boldsymbol{v} = [\boldsymbol{v}_B{}^T, \boldsymbol{v}_N{}^T]^T$ in accordance with $\boldsymbol{q} = [\boldsymbol{q}_B{}^T, \boldsymbol{q}_N{}^T]^T$. Using $v_i = q_i/A_i$ for each $i \in I$, we can write

$$\begin{aligned} \boldsymbol{v}_N &= \boldsymbol{D}_N^{-1}\boldsymbol{q}_N = \boldsymbol{D}_N^{-1}\boldsymbol{A}_N^{-1}(\boldsymbol{b} - \boldsymbol{A}_B\boldsymbol{q}_B) \\ &= \boldsymbol{D}_N^{-1}\boldsymbol{A}_N^{-1}(\boldsymbol{b} - \boldsymbol{A}_B\boldsymbol{D}_B\boldsymbol{v}_B), \end{aligned} \tag{2a}$$

where $\boldsymbol{D}_N \in \mathbb{R}^{(n-1)\times(n-1)}$ is a diagonal matrix with j^{th} diagonal entry $\boldsymbol{D}_N(j, j) = A_i$, v_i corresponds to the jth component of $\boldsymbol{v}_N$, $\boldsymbol{D}_B \in \mathbb{R}^{(m+1)\times(m+1)}$ is a diagonal matrix with j^{th} diagonal entry $\boldsymbol{D}_B(j, j) = A_i$, and v_i corresponds to the jth component of $\boldsymbol{v}_B$.

By the incompressibility of airflow under low Mach number, a similar formula holds for the airflow acceleration:

$$\dot{\boldsymbol{v}}_N = \frac{d\boldsymbol{v}_N}{dt} = -\boldsymbol{D}_N^{-1}\boldsymbol{A}_N^{-1}\boldsymbol{A}_B\boldsymbol{D}_B\dot{\boldsymbol{v}}_B. \tag{2b}$$

Let us now reveal key aspects of the structure of the linear dependencies given in (2). By inspection of (1) in the proof of Lemma 1, we know that $\boldsymbol{A}$ has entry values in $\{0, 1, -1\}$, so $\boldsymbol{B} = \boldsymbol{A}_N{}^{-1}\boldsymbol{A}_B \in \mathbb{R}^{(n-1)\times(m+1)}$ also has entry values in $\{0, 1, -1\}$. Specifically, (1) implies that for all i, j with $1 \le i \le n - 1$ and $1 \le j \le m + 1$,

$$\boldsymbol{B}(i, j) = \begin{cases} 1, & \text{if } j = 1 \text{ or } j - 1 \in I_{\text{in}}; \\ -1, & \text{if } j - 1 \in I_{\text{out}}; \\ 0, & \text{otherwise.} \end{cases} \tag{3a}$$

Since the cross-sectional areas A_i ($i \in I$) are positive, the diagonal matrices $\boldsymbol{D}_B$ and $\boldsymbol{D}_N{}^{-1}$ just scale the entries of $\boldsymbol{B}$ up and down, without changing their signs. Let $\boldsymbol{C} = \boldsymbol{D}_N{}^{-1}\boldsymbol{B}\boldsymbol{D}_B$. Then for all i', j' with $1 \le i' \le n - 1$, and $1 \le j' \le m + 1$, we have

$$\boldsymbol{C}(i, j) = \begin{cases} \alpha_{i'j'}, & \text{if } j' = 1 \text{ or } j' - 1 \in I_{in}; \\ -\alpha_{i'j'}, & \text{if } j' - 1 \in I_{out}; \\ 0, & \text{otherwise.} \end{cases} \tag{3b}$$

where $\alpha_{i'j'} = A_{j'}/A_{i'} > 0$, segment i' corresponds to the ith element of I_N, and j' corresponds to the jth element of I_B. Recall that $I_B = \{1, n + 1, n + 2, \ldots, n + m\}$ and $I_N = \{2, 3, \ldots, n\} = \{2, 3, \ldots, h_1, h_1 + 1, \ldots, h_2, \ldots, h_{m-1} + 1, \ldots, h_m, h_m + 1, \ldots, n\}$. Therefore,

$$\boldsymbol{C} = \begin{bmatrix} \boldsymbol{\alpha}_{01} & \boldsymbol{0} & \boldsymbol{0} & \boldsymbol{0} & \cdots & \boldsymbol{0} \\ \boldsymbol{\alpha}_{11} & \pm\boldsymbol{\alpha}_{1,n+1} & \boldsymbol{0} & \boldsymbol{0} & \cdots & \boldsymbol{0} \\ \boldsymbol{\alpha}_{21} & \pm\boldsymbol{\alpha}_{2,n+1} & \pm\boldsymbol{\alpha}_{2,n+2} & \boldsymbol{0} & \cdots & \boldsymbol{0} \\ \vdots & \vdots & \vdots & \vdots & \ddots & \vdots \\ \boldsymbol{\alpha}_{m1} & \pm\boldsymbol{\alpha}_{m,n+1} & \pm\boldsymbol{\alpha}_{m,n+2} & \pm\boldsymbol{\alpha}_{m,n+3} & \cdots & \pm\boldsymbol{\alpha}_{m,n+m} \end{bmatrix}, \tag{3c}$$

where $\boldsymbol{\alpha}_{jj'}$ is the vector $[\alpha_{h_{j+1}j'}, \ldots, \alpha_{h_{j+1}j'}]^T$, $j = 1, \ldots, m$; the sign of $\boldsymbol{\alpha}_{jj'}$ is positive if $j' = 1$ or $j' \in I_{\text{in}}$, and negative if $j' \in I_{\text{out}}$.

Let $\boldsymbol{S} = [\boldsymbol{I}\ \ -\boldsymbol{C}^T]^T$ and $\boldsymbol{s} = [\boldsymbol{0}^T\ \ (\boldsymbol{D}_N{}^{-1}\boldsymbol{A}_N{}^{-1}\boldsymbol{b})^T]^T$. Then we can write (2a) and (2b) as follows:

$$\begin{cases} \boldsymbol{v} = [\boldsymbol{v}_B, \boldsymbol{v}_N]^T = \boldsymbol{S}\boldsymbol{v}_B + \boldsymbol{s}; \\ \dot{\boldsymbol{v}} = [\dot{\boldsymbol{v}}_B, \dot{\boldsymbol{v}}_N]^T = \boldsymbol{S}\dot{\boldsymbol{v}}_B. \end{cases} \tag{4}$$

The purpose of this split is to build a compact aerodynamic-system model that, given all the design parameters such as the numbers of operating fans and vents, keeps track of only the basic velocity variables (the ones in $\boldsymbol{v}_B = \{v_i, i \in I_B\}$) and their derivatives.

C. Aerodynamic equations

Now we establish the basic set of aerodynamic equations of a bifurcate tunnel system. We start with the force balance equation in each tunnel segment [11], [15], [20]:

$$\rho AL\dot{v} = \sum F = F_f + F_t + F_r + F_e, \tag{5a}$$

where ρ is the air density (kg/m^3), A is the cross-sectional area of the tunnel segment (m^2), L is the longitudinal length of the segment (m), and ΣF is the sum of the external forces (kN) imposed on the air in the segment, which consists of four parts:

(i). Fan thrust F_f:

$$F_f = N\rho K A_f v_f (v_f - v), \tag{5b}$$

where N is the number of running jet fans in the segment; K is the pressure-rise coefficient that depends on the specification parameters of the jet fans [25] and is independent of traffic intensity [11]; A_f and v_f are the cross-sectional area (m^2) and jet speed (m/s) of the jet fans, respectively. In general, $v_f >> v$.

(ii). Traffic force F_t:

$$F_t = \frac{\rho L V_t A_v}{2 v_t}(v_t - v)|v_t - v|, \tag{5c}$$

where V_t is the traffic volume (veh/s), v_t is the average speed (m/s) of the vehicles in the tunnel segment, and A_v is the equivalent average vehicle frontal area (with multiplicative drag coefficient included) in the segment (m^2). Note that traffic can also constitute a resistance to airflow (i.e., $F_t < 0$) when $v_t < v$ (e.g., during congested traffic). Here (5c) is for a one-way traffic tunnel; it can be extended to a two-way traffic tunnel by adding a similar force term which is caused by traffic flow in the direction opposite that of the airflow [20], [26]. Typically, the traffic volume changes on a time scale which is much longer than that of the transient airflow [4] [13], hence the traffic parameters are assumed constant in our steady-state analysis.

(iii). Frictional resistance (and local pressure loss) F_r:

$$F_r = -\frac{\rho}{2} A(\lambda \frac{L}{d_e} + \xi) v^2, \tag{5d}$$

where λ is the coefficient of friction resistance of the tunnel wall; d_e is the hydraulic diameter of the tunnel segment (m); and ξ is the local pressure-loss coefficient, which may consist of two parts [20]: a flow-independent loss coefficient ζ^0 and a flow-dependent loss coefficient ζ. In that case, $\xi = \zeta^0 + \zeta$. For instance, the pressure-loss coefficient of the inlet/outlet or of the flow expansion/contraction (changes in cross-sectional shape), and the pressure-loss coefficient of the longitudinal curvature, are routinely regarded as flow-independent [20], hence they can be determined exogenously and are positive. However, the pressure-loss coefficients of flows at the tunnel junctions are flow-dependent [9] [20] and can be negative. We will discuss the determination of ζ in detail later.

For simplicity, we neglect pressure losses at upper vents (if any), since the airflow through these vents is typically very small compared to the original airflow inside the tunnel [4]. However, the entire analysis in this paper can easily be extended to consider (both constant and flow-dependent) pressure-loss coefficients at the upper vents.

(iv). Boundary pressure difference F_e:

$$F_e = A(p_{\text{in}} - p_{\text{out}}), \tag{5e}$$

where $p_{\text{in}} \geq 0$, $p_{\text{out}} \geq 0$ are the static pressure (kPa) at the airflow-in and airflow-out points of the segment, respectively.

Applying (2) to all the tunnel segments $i \in I$, we can write

$$\begin{cases} L_i \dot{v}_i = g_i(v_i) + \frac{p_{i-1}}{\rho} - \frac{p_i}{\rho}, (i = 1, ..., n); \\ L_i \dot{v}_i = g_i(v_i) - \frac{p_j}{\rho}, (i \in I_{\text{in}}, j = h_i); \\ L_i \dot{v}_i = g_i(v_i) + \frac{p_j}{\rho}, (i \in I_{\text{out}}, j = h_i), \end{cases} \tag{6a}$$

where p_i is the static pressure p_{out} for segment i and p_{in} is the static pressure for segment $i + 1$; p_{out} and p_{in} are as defined in (5e). The static pressure at the tunnel portals is 0; in particular, $p_0 = p_n = 0$; also, $p_{\text{in}} = 0$ for every segment $i \in I_{\text{in}}$, and $p_{\text{out}} = 0$ for every segment $i \in I_{\text{out}}$. $g_i(v_i) = a_i v_i^2 + b_i v_i + c_i$ is a quadratic function, with coefficients given below (where the subscript i is omitted on variables that are constant across different segments):

$$\begin{cases} a_i = \frac{\text{sgn}(v_{ti} - v_i) V_{ti} A_{vi}}{2 A_i v_{ti}} - \frac{\lambda}{2 d_{ei}} - \frac{\xi_i}{2 L_i}; \\ b_i = -\left(\frac{N_i A_f K v_f}{A_i L_i} + \frac{\text{sgn}(v_{ti} - v_i) V_{ti} A_{vi}}{A_i} \right); \ i \in I. \\ c_i = \frac{N_i A_f K v_f^2}{A_i L_i} + \text{sgn}(v_{ti} - v_i) \frac{V_{ti} A_{vi} v_{ti}}{2 A_i}, \end{cases} \tag{6b}$$

where the sign function sgn(x) = -1, 0, 1 when $x < 0$, $= 0$, > 0, respectively, which encodes (5c).

D. Air Pollutant Dispersion Model

The distribution of air pollutant concentration inside a longitudinally ventilated tunnel can be described by one-dimensional diffusion-advection equations [13]. Pollutant deposition is neglected due to its limited effect on the dispersion and movement of gaseous pollutants inside the tunnel [21]. As a result, for each tunnel segment $i \in I$ we have:

$$\frac{\partial c_i^p}{\partial t} = \frac{\partial}{\partial x_i}\left(k_x \frac{\partial c_i^p}{\partial x_i} \right) - v_i \frac{\partial c_i^p}{\partial x_i} + e_i^p \tag{7a}$$

where c^p_i is concentration of pollutant p in segment i (mg/m^3), x_i is the distance from the starting point of segment i (m), k_x is the longitudinal diffusion coefficient (m^{-2}), e^p_i is the emission rate of pollutant p (mg/m^3/s), which is the emission from running vehicles in tunnel segment i. Given that advection and source emissions dominate the distribution of pollutant concentrations in the tunnel [27], (7a) can be simplified by dropping the diffusion term. Hence the steady-state solution to the simplified tunnel diffusion-advection equation takes the form:

$$c_i^p(x_i) = c_{0i}^p + \frac{e_i^p x_i}{v_i^*}, \tag{7b}$$

where v_i^* is the stable equilibrium air-velocity in segment i; c^p_{0i} is the concentration of pollutant p at the upstream end of segment i (mg/m^3), which depends on the pollution level, upper vents, and ramp accesses in the upstream segments. c^p_{0i} can be determined for different types of tunnel segments as below.

For the mainline entrance segment and the on-ramps that are inlets of traffic:

$$c_{0i}^p = c_{amb,i}^p, \ i = 1 \text{ or } i \in I_{in}. \tag{7c}$$

where $c^p_{amb,i}$ is the ambient pollutant concentration outside the tunnel segment i (mg/m^3). For off-ramps,

$$c^p_{0j} = c^p_i(L_i),\ i = h_j,\ j \in I_{in}. \tag{7d}$$

For two adjacent mainline segments divided by an air extraction vent or an off-ramp access point,

$$c^p_{0i+1} = c^p_i(L_i),\ i = 1,\ldots,n-1 \text{ s.t. } q'_i < 0 \text{ or } i \in I^{main}_{out}. \tag{7e}$$

For two adjacent mainline segments divided by an air supplement vent, by conservation of mass [21], we have

$$c^p_{0i+1} = \frac{v^*_i A_i c^p_i(L_i) + q'_i\, c^p_{amb,i}}{v^*_i A_i + q'_i},\ i = 1,\ldots,n-1 \text{ s.t. } q'_i > 0. \tag{7f}$$

Finally, for two adjacent mainline segments divided by the access point of an on-ramp,

$$c^p_{0i+1} = \frac{v^*_i A_i c^p_i(L_i) + v^*_{n+j} A_{n+j} c^p_{n+j}(L_{n+j})}{v^*_i A_i + v_{n+j} A_{n+j}},\ i = h_j,\ j \in I_{in}. \tag{7g}$$

Therefore, if we can determine the stable equilibrium velocities $\{v_i^*\}$, then we are able to easily compute the steady-state pollutant concentrations over all the segments based on recursion (7). In the following two sections we will focusing on analyzing steady-state flows and their stability.

III. Flow-Dependent Local Pressure-Loss Coefficients and PWA Approximation

A. Local pressure-loss coefficients at tunnel junctions

Given the required ventilation direction in each tunnel segment, our goal is to determine the steady-state flow pattern in the system. In junctions of bifurcate tunnels, given the tunnel geometric layout, the local pressure-loss coefficient depends on the relative relationships among the mainline flows upstream and downstream of the junction and the flow in the lateral branch. These coefficients can even be negative under certain flow ratios and cross-sectional area ratios [9].

We assume that the ventilation direction throughout the mainline or single-branch tunnel is unidirectional, since we focus on normal operation. In the case of a fire in which the fire point is near the tunnel air inlet, the fans in the upstream part of the fire point may be reversed in order to block transport of the smoke to the other part of the tunnel and enable evacuation [5], [20]. In any case, the airflow in each lateral branch either joins to or separates from the mainline airflow.

For typical settings, where the mainline tunnel is straight and has constant cross-sectional area at the junctions, these tunnel junctions have two possible flow types, as depicted in Table I. The corresponding analytical formulae for the pressure-loss coefficients, which are based on [9], are listed in Table I. It is important to note that these analytical formulae are derived on the basis of a steady flow; however, it is normally assumed that when there is an unsteady flow, the pressure loss between any two branches of the junction is instantaneously equivalent to that occurs in the case of steady flow [9]. Extensive numerical studies have shown that steady-flow coefficients can be used in the case of unsteady flow without compromising accuracy [9].

We assume that the mainline cross-sectional area at a junction (associated with ramp j) is η_j times the cross-sectional area of the lateral branch segment $n + j$ at this junction. Note that the loss coefficients apply only to the two segments where the flow joins to a downstream "common" flow or separates from an upstream "common" flow. For example, in a type-I junction, ζ_1 applies to segment 1 and ζ_2 applies to segment 2, while segment 3 does not have local pressure loss.

Note that the formulae presented in Table I are just for "T-junctions" with constant mainline cross-sectional areas upstream and downstream of the junction. Some tunnels may have a more complicated junction layout, for example, if the mainline cross-sectional areas upstream and downstream of the junction are different, more than two branches connect to the junction, or there is a non-straight/curved mainline alignment over the junction region that forms a "Y-junction." In these cases, explicit analytical formulae are hard to obtain. A more common approach is via experimental measurement or CFD analysis [5], [7].

The true functional forms of these local loss coefficients should all be nonlinear in the flow-ratios, which makes the analysis of an aerodynamic model cumbersome. Therefore, we seek a proper approximation of these functions that will enable a more convenient analysis. Given the other tunnel parameters, all these functions are smooth in the flow-ratio variables. For instance, it can be checked that each ζ is a smooth function of the corresponding flow-ratio variable $r \in [\delta,\ 1-\delta]$ as defined in Table I. Thus a high-precision approximation is possible, which makes the resultant steady-state analysis meaningful for practical purposes.

TABLE I
Two Types of Junctions and Local Pressure-Loss Coefficients

Type of junction	Flow ratio $r \in [\delta, 1-\delta]$[a]	Analytical formulae for local pressure-loss coefficients [9]
Type I 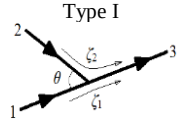	$r_1 = \frac{v_1}{v_3}$	$\zeta_1 = \frac{2\eta[1-r_1-(1-r_1)^2\eta\cos\theta]}{\eta+0.5\cos\theta} + r_1 - 1,\ \theta \le \frac{\pi}{2}$ $\zeta_1 = 1 - r_1 + 2(1-r_1)^2\eta\cos\theta,\ \theta > \frac{\pi}{2}$
	$r_2 = \frac{v_2}{\eta v_3}$	$\zeta_2 = \frac{2\eta[r_2(2-r_2)-r_2\eta\cos\theta]}{\eta+0.5\cos\theta} + \eta^2 r_2 - 1,\ \theta \le \frac{\pi}{2}$ $\zeta_2 = 4r_2 - 1 + r_2(\eta^2 + 2\eta\cos\theta - 2),\ \theta > \frac{\pi}{2}$
Type II 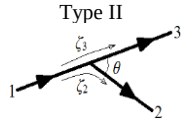	$r_3 = \frac{v_3}{v_1}$	$\zeta_3 = r_3^2 - 1.5r_3 + 0.5$
	$r_2 = \frac{v_2}{\eta v_1}$	$\zeta_2 = \eta^2 r_2^2 - 2\eta r_2\cos(0.75\theta) + 1,\ \theta \le \frac{\pi}{2}$ $\zeta_2 = \eta^2 r_2 - 2\eta r_2\cos(\pi - 0.75\theta) + 1,\ \theta > \frac{\pi}{2}$

[a] In general, each flow ratio r can be in the range [0, 1]; see [9]. Since in practice $v_i > 0$, we restrict r to the interval $[\delta, 1-\delta]$, with $\delta > 0$ chosen to be a small number (e.g., 0.01). This enables us to work with the reciprocals of the squares of the flow ratios, which is very convenient when incorporating them into the aerodynamic equations. This will become clear in Section IV.

B. Piecewise-affine approximation

We introduce a piecewise-affine (PWA) approximation to the analytical formulae for the local pressure-loss coefficients. In fact, arbitrary approximation bounds can be achieved by a properly chosen PWA function in terms of the reciprocal of the square of the flow ratio.

Lemma 2: Suppose $\zeta = \zeta(r)$ is smooth on $[\delta,\ 1-\delta]$. Then for any $\varepsilon > 0$, there exists a PWA function $\hat{\zeta}$ such that

$$|\hat{\zeta}(f(r))-\zeta(r)|\le \varepsilon,\ \ \forall r\in[\delta,1-\delta],$$

where $f(r) = r^{-2}$.

Proof: Since $f(r)$ is bijective on $[\delta, 1-\delta]$, we define $\zeta^s = \zeta^s(f(r)) = \zeta^s(r^2) = \zeta(r)$. The smoothness of $\zeta = \zeta(r)$ indicates that it is Lipschitz continuous on $[\delta, 1-\delta]$ and that the function $f(r)$ is also Lipschitz continuous on $[\delta, 1-\delta]$, hence so is their composition, $\zeta^s(f(r))$. Therefore, we can assume that for any $r, r' \in [\delta, 1-\delta]$ such that $r \ne r'$,

$$\max_{r_j\ne r_{j'}\in(0,1)}\frac{|\zeta^s(r^{-2})-\zeta^s((r')^{-2})|}{|r-r'|}=\frac{|\zeta(r)-\zeta(r')|}{|r-r'|}=\Delta.$$

For a fixed $\varepsilon > 0$, if we choose the interval division points of the PWA function as $\delta = r^{(0)}, r^{(1)}, r^{(1)}, r^{(2)}, \ldots, r^{(M-1)}, r^{(M)} = 1-\delta$ such that $\hat{\zeta}(r^{(t)-2}) = \zeta^s(r^{(t)-2}) = \zeta(r^{(t)})$, $t = 1, \ldots, M$, and

$$\max_{t=1,\ldots N}|r^{(t)}-r^{(t-1)}|\le\frac{\varepsilon}{\Delta},$$

then the PWA function has the desired property. This is because the approximation function is affine on $[r^{(t-1)}, r^{(t)}]$ and its function values at the two endpoints are equal to the true values. Thus for any $\bar{r} \in [r^{(t-1)}, r^{(t)}]$,

$$\begin{aligned}|\hat{\zeta}(\bar{r}^{-2})-\zeta(\bar{r})| &\le \max\{|\hat{\zeta}(r^{(t)-2})-\zeta(\bar{r})|,|\hat{\zeta}(r^{(t-1)-2})-\zeta(\bar{r}))|\}\\ &=\max\{|\zeta(r^{(t)})-\zeta(\bar{r})|,|\zeta(r^{(t-1)})-\zeta(\bar{r})|\}\\ &\le|\zeta(r^{(t)})-\zeta(r^{(t-1)})|\\ &\le\Delta\cdot\varepsilon/\Delta=\varepsilon,\end{aligned}$$

which holds for $t = 1, \ldots, M$.

■

Given the type of junction associated with ramp segment $n + j$, $j \in \{1, \ldots, m\}$, and the corresponding mainline segments h_j, $h_j + 1$ upstream and downstream of the junction, there are two flow-dependent local pressure-loss coefficients: If $j \in I_{\text{in}}$, then the junction is of type I, so the coefficients ζ_{n+j} and ζ_{h_j} are applied to segments $n + j$ and h_j, respectively; if $j \in I_{\text{out}}$, then the junction is of type II, so the coefficients ζ_j and ζ_{h_j+1} are applied to segments $n + j$ and $h_j + 1$, respectively.

Note that our modeling goal is to describe the flow in terms of only the velocity variables, so we need to eliminate the boundary pressure terms for all the segments. Because of the coupling of the aerodynamic equations (6a) for segments j, h_j, and $h_j + 1$ which is due to the common boundary pressure p_{h_j}, eliminating p_{h_j} will include both ζ_{h_j} and ζ_{n+j} (for $j \in I_{\text{in}}$) or both ζ_{h_j+1} and ζ_{n+j} (for $j \in I_{\text{out}}$) in the equations. Therefore, to establish a system of simultaneous equations in the velocity variables that uses fixed affine approximation functions for the ζ's in a certain range of the flow ratio for each junction, we need PWA functions for which the two loss coefficients at each junction are compatible. Let $\boldsymbol{r}_j = [r_j^{(0)}, r_i^{(1)}, \ldots, r_i^{(M_i)}]^T$ (where $r_i^{(0)} = \delta$ and $r_i^{(M_i)} = 1-\delta$) be the division points of the PWA function for ζ_i. By "compatible," we mean that for $j \in I_{\text{in}}$, $M_j = M_{h_j}$ and $r_j^{(t)} + r_{h_j}^{(t)} = 1$, $t = 1, \ldots, M_j$; and for $j \in I_{\text{out}}$, $M_j = M_{h_j+1}$ and $r_j^{(t)} + r_{h_j+1}^{(t)} = 1$, $t = 1, \ldots, M_j$. To see that this relationship is valid, note that $r_1 + r_2 = 1$ for a type-I junction and $r_3 + r_2 = 1$ for a type-II junction, as can be seen in Table I.

For each local pressure-loss coefficient ζ_i ($i \in I_{\text{in}}^{\text{main}} \cup I_{\text{out}}^{\text{main}} \cup \{n + 1, \ldots, n + m\}$, we partition the interval $[\delta, 1-\delta]$ into M_i pieces: $[r_i^{(0)}, r_i^{(1)})$, $[r_i^{(1)}, r_i^{(2)})$, …, $[r_i^{(M_i-1)}, r_i^{(M_i)}]$, with $r_i^{(0)} = \delta$ and $r_i^{(M_i)} = 1-\delta$. Thus for every j in $\{1, \ldots, m\}$, and for $i = h_j$ if $j \in I_{\text{in}}$ and $i = h_j + 1$ if $j \in I_{\text{out}}$, the corresponding PWA function has the following form:

$$\begin{cases}\hat{\zeta}_i=\sum_{t=1}^{N_j}H_j^{(t)}(\alpha_i^{(t)}+\beta_i^{(t)}r_i^{-2});\\ \hat{\zeta}_{n+j}=\sum_{t=1}^{N_j}H_j^{(t)}(\alpha_j^{(t)}+\beta_j^{(t)}r_j^{-2}),\end{cases}$$
$$H_j^{(t)}=\begin{cases}1, & \text{if } r_j\in[r_j^{(t-1)},r_j^{(t)});\\ 0, & \text{otherwise},\end{cases}\quad t=1,\ldots,M_j-1 \tag{8a}$$
$$H_j^{(M_j)}=\begin{cases}1, & \text{if } r_j\in[r_j^{(M_j-1)},r_j^{(M_j)}];\\ 0, & \text{otherwise}.\end{cases}$$

Note that the PWA function is continuous, which implies that $\alpha_i^{(t)} + \beta_i^{(t)} r_j^{(t)-2}$ for every t in $\{0, \ldots, M_j - 1\}$.

C. *Fitting the piecewise-affine functions*

We consider the commonly used criteria [28] for fitting our PWA function defined in (8a): Given the preferred number of pieces, the PWA function should minimize the total error (i.e., the deviation from the true nonlinear function). Under this criterion, one approach is to fit a PWA function to the values of r_i for the individual tunnel junctions by minimizing the error of each function separately, and then generate a set of compatible division points based on the distinct endpoints in each piece of the PWA function and their *compatible* counterparts (i.e., $r_j = 1 - r_i$). However, this is not efficient and may lead to an unnecessarily large number of pieces. Instead, we choose to set the division points and the affine function parameters by solving a least-squares (LS) problem. Given $M_j \ge 1$, we formulate the following problem for every j in $\{1, \ldots, m\}$:

$$\begin{aligned}&\min_{r_j,\boldsymbol{\alpha}_i,\boldsymbol{\alpha}_j}\int_{\delta}^{1-\delta}w_i(\mu)[\hat{\zeta}_i(\mu^{-2})-\zeta_i(\mu)]^2+w_j(\mu)[\hat{\zeta}_j(\mu^{-2})-\zeta_j(\mu)]^2\,d\mu\\ &\text{s.t. }\hat{\zeta}_i(\mu^{-2})=\alpha_i^{(t)}+\beta_i^{(t)}(\mu-r_i^{(t-1)-2}),\ \mu\in[r_i^{(t-1)},r_i^{(t)}],\ t=1,\ldots,M_j,\\ &\qquad\hat{\zeta}_i(\mu^{-2})=\alpha_j^{(t)}+\beta_j^{(t)}(\mu-r_j^{(t-1)-2}),\ \mu\in[r_j^{(t-1)},r_j^{(t)}],\ t=1,\ldots,M_j\\ &\qquad\beta_i^{(t)}=\frac{\zeta_i(r_i^{(t)})-\zeta_i(r_i^{(t-1)})}{r_i^{(t)-2}-r_i^{(t-1)-2}};\ \beta_j^{(t)}=\frac{\zeta_j(r_j^{(t)})-\zeta_j(r_j^{(t-1)})}{r_j^{(t)-2}-r_j^{(t-1)-2}}\\ &\qquad\boldsymbol{r}_i=\mathbf{1}-\boldsymbol{r}_j,\ r_j^{(0)}=\delta,\ r_j^{(M_j)}=1-\delta\end{aligned} \tag{8b}$$

where $\boldsymbol{\alpha}_i$ and $\boldsymbol{\alpha}_j$ are the vectors $\{\alpha_i^{(t)}\}$ and $\{\alpha_j^{(t)}\}$, respectively, w_i and w_j are the corresponding weighting functions, and $\mathbf{1}$ is a column vector of ones. Note that in (8b) only the intercepts $\boldsymbol{\alpha}_i$, $\boldsymbol{\alpha}_j$ and the intermediate components of $\boldsymbol{r}_j$ need to be optimized, since $\boldsymbol{r}_j$ and $\boldsymbol{r}_i$ are compatible and the PWA functions are continuous. This LS problem can be solved efficiently by methods such as the multi-start Gauss–Newton algorithm [29].

If an analytical form $\zeta(r)$ is not available and we have only discrete observations of the function values, then the integral of the objective function of (8b) can be replaced by a summation. The problem can be formulated as an LS-based piecewise-linear regression. A simple heuristic for this problem is to choose the endpoints among the data points that minimize the sum of the errors over all the data points.

IV. Steady-State Airflow And Its Stability

To simplify the analysis, in what follows we assume:

Assumption 1: Throughout the system, the air velocity does not exceed the traffic speed, i.e., $v_i \le v_{ti}$ for all $i \in I$.

Assumption 1 generally holds under normal traffic. The derivation can easily be extended to the case where the relation between v_i and v_{ti} is unrestricted. The extension can be done by including possible combinations of these relations over all $i \in I$ in determining the system parameters (see (6b)).

A. System of ODEs in basic velocity variables

The ultimate goal of aerodynamic modeling is to create a compact system of first-order ODEs in terms of $\boldsymbol{v}_B$ and compute its solutions in the feasible region. We denote the feasible region of $\boldsymbol{v}_B$ by V. In our problem, due to the restrictions on $\boldsymbol{v} = [\boldsymbol{v}_B, \boldsymbol{v}_N]^T \in \mathbb{R}_+^{n+m}$ and $r_j \in [\delta, 1-\delta]$, we have $r_{h_j} \in [\delta, 1-\delta]$ for all j in $\{1, \ldots, m\}$. Thus V is defined as follows:

$$V = \{\boldsymbol{v}_B : \boldsymbol{P}\boldsymbol{v}_B \ge \boldsymbol{p}\};\ \boldsymbol{P} = \begin{bmatrix} \boldsymbol{S} \\ -\boldsymbol{S} \\ \boldsymbol{MS} \end{bmatrix};\ \boldsymbol{p} = \begin{bmatrix} -\boldsymbol{s} \\ \boldsymbol{s} - \boldsymbol{v}_t \\ \boldsymbol{Ms} \end{bmatrix}, \tag{9}$$

where $\boldsymbol{v}_t$ is the vector $\{\boldsymbol{v}_{ti}, i \in I\}$, $\boldsymbol{S}$ and $\boldsymbol{s}$ are defined as in (4), and the matrix $\boldsymbol{M} \in \mathbb{R}^{2m\times(n+m)}$ encodes the constraints $\delta \le r_j \le 1-\delta$, $j = 1, \ldots, m$. Note that under these constraints, the conditions $\delta \le r_{h_j} \le 1-\delta$ for $j \in I_{\text{in}}$ and $\delta \le r_{h_j+1} \le 1-\delta$ for $j \in I_{\text{out}}$ hold automatically. Specifically, suppose components i, i', and i'' of $\boldsymbol{v}$ correspond to v_j, v_{h_j} and v_{h_j+1}, respectively. Then $\boldsymbol{M}(2j-1, i) = 1$ and $\boldsymbol{M}(2j, i) = -1$. In addition, if $j \in I_{\text{in}}$, then $\boldsymbol{M}(2j-1, i'') = -\delta\eta_j$ and $\boldsymbol{M}(2j, i'') = (1-\delta)\eta_j$; and if $j \in I_{\text{out}}$, then $\boldsymbol{M}(2j-1, i') = -\delta\eta_i$ and $\boldsymbol{M}(2j, i') = (1-\delta)\eta_j$. The other entries of $\boldsymbol{M}$ are all zeros.

Clearly, V is a polyhedron. We can further partition V into disjoint convex sub-regions. Given the partition points $\boldsymbol{r}_j$ of the PWA functions at each tunnel junction associated with ramp segment $n + j \in \{n+1, \ldots, n+m\}$ with $|\boldsymbol{r}_j| = M_j$, we can partition the feasible region $\mathbb{R}_+^{m+1}$ into a total of $M = |M_1| \times |M_2| \times \ldots \times |M_m|$ convex sets. This is because for each $i \in \{n+1, \ldots, n+m\}$, there can be only one indicator function among $\{H_i^{(t)}, t = 1, \ldots, M_i\}$ that takes the value 1; the others are all 0. Thus altogether we have M different combinations of active indicator functions among all m tunnel junctions. The convexity of the partition follows by the following lemma:

Lemma 3: The set $V_k = \{\boldsymbol{v}_B \in V: H_j^{(t_j)} = 1, j = 1, \ldots, m\}$ is convex.

Proof: By definition of $H_j^{(t_j)}$, we know that $H_j^{(t_j)} = 1$ implies: (i) $r_i \in [r_j^{(t_j-1)}, r_j^{(t_j)})$ for $t_j = 1, \ldots, M_j - 1$ and (ii) $r_i \in [r_j^{(t_j-1)}, r_j^{(t_j)}]$ for $t_j = M_j$. This amounts to linear constraints on $\boldsymbol{v}_B$: $\boldsymbol{N}_1(\boldsymbol{S}\boldsymbol{v}_B + \boldsymbol{s}) \ge \boldsymbol{0}$ and $\boldsymbol{N}_2(\boldsymbol{S}\boldsymbol{v}_B + \boldsymbol{s}) > \boldsymbol{0}$, where $\boldsymbol{N}_1$ and $\boldsymbol{N}_2$ encode (i) and (ii), respectively, and both of them can be defined in a way that is similar to $\boldsymbol{M}$ in (9). Thus, $V' = \{\boldsymbol{v}_B: \boldsymbol{N}_1(\boldsymbol{S}\boldsymbol{v}_B + \boldsymbol{s}) \ge \boldsymbol{0}, \boldsymbol{N}_2(\boldsymbol{S}\boldsymbol{v}_B + \boldsymbol{s}) > \boldsymbol{0}\}$ is convex, and since V is convex, so is $V_k = V \cap V'$. ■

Thus, we have M disjoint convex sets $V_1, \ldots, V_N$ that form a partition of V. Based on the PWA function in (8a), the system of aerodynamic equations (6) turns out to be a nice structured system of ODEs in the basic velocity variables $\boldsymbol{v}_B$ within each subset V_k ($k = 1, \ldots, M$).

Proposition 1: If the local pressure-loss coefficients ζ are replaced by their approximations $\hat{\zeta}$ in (8a), then for $\boldsymbol{v}_B \in V_k$ the system (6) is equivalent to the following ODE with quadratic polynomials $\boldsymbol{F}^{(k)}$ in $\boldsymbol{v}_B$:

$$\dot{\boldsymbol{v}}_B = \boldsymbol{\Lambda}^{-1}\begin{bmatrix} \boldsymbol{v}_B^T\boldsymbol{X}_1^{(k)}\boldsymbol{v}_B + \boldsymbol{y}_1^{(k)T}\boldsymbol{v}_B + z_1^{(k)} \\ \boldsymbol{v}_B^T\boldsymbol{X}_2^{(k)}\boldsymbol{v}_B + \boldsymbol{y}_2^{(k)T}\boldsymbol{v}_B + z_2^{(k)} \\ \vdots \\ \boldsymbol{v}_B^T\boldsymbol{X}_{m+1}^{(k)}\boldsymbol{v}_B + \boldsymbol{y}_{m+1}^{(k)T}\boldsymbol{v}_B + z_{m+1}^{(k)} \end{bmatrix} = \boldsymbol{F}^{(k)}(\boldsymbol{v}_B), \tag{10}$$

where $\boldsymbol{\Lambda} \in \mathbb{R}^{(m+1)\times(m+1)}$ is a nonsingular matrix, $\boldsymbol{X}^{(k)}_1, \ldots, \boldsymbol{X}^{(k)}_{m+1} \in \mathbb{R}^{(m+1)\times(m+1)}$ are symmetric matrices, $\boldsymbol{y}^{(k)}_1, \ldots, \boldsymbol{y}^{(k)}_{m+1} \in \mathbb{R}^{(m+1)}$, and $z^{(k)}_1, \ldots, z^{(k)}_{m+1} \in \mathbb{R}$, these quantities take the values in (A5).

Proof: See the Appendix. ■

Proposition 1 is a starting point for analyzing steady-state flow patterns and their stabilities for bifurcate tunnels.

B. Solving for the steady-state flow

By Proposition 2 and since $\boldsymbol{\Lambda}$ is nonsingular, computing the steady-state solution of (10) amounts to solving M systems of quadratic equations, each within a convex set V_k ($k = 1, \ldots, M$):

$$\begin{cases} \boldsymbol{v}_B^T\boldsymbol{X}_1^{(k)}\boldsymbol{v}_B + \boldsymbol{y}_1^{(k)T}\boldsymbol{v}_B + z_1^{(k)} = 0; \\ \boldsymbol{v}_B^T\boldsymbol{X}_2^{(k)}\boldsymbol{v}_B + \boldsymbol{y}_2^{(k)T}\boldsymbol{v}_B + z_2^{(k)} = 0; \\ \vdots \\ \boldsymbol{v}_B^T\boldsymbol{X}_{m+1}^{(k)}\boldsymbol{v}_B + \boldsymbol{y}_{m+1}^{(k)T}\boldsymbol{v}_B + z_{m+1}^{(k)} = 0. \end{cases} \tag{11}$$

We can write (11) in the abstract form $Q^{(k)}(\boldsymbol{v}_B) = \boldsymbol{0}$, where $Q^{(k)}$ is a quadratic operator from $\mathbb{R}^{(m+1)}$ to $\mathbb{R}^{(m+1)}$. Based on the proof of Proposition 1 (in the Appendix), we can express the coefficients in the jth equation ($j = 1, \ldots, m+1$) in (11) as

$$\begin{cases} \boldsymbol{X}_j^{(k)} = \boldsymbol{S}^T\boldsymbol{D}_j^{(k)}\boldsymbol{S}; \\ \boldsymbol{y}_j^{(k)} = \boldsymbol{S}^T(2\boldsymbol{D}_j^{(k)}\boldsymbol{s} + \boldsymbol{w}_j); \\ z_j^{(k)} = (\boldsymbol{s}^T\boldsymbol{D}_j^{(k)} + \boldsymbol{w}_j^T)\boldsymbol{s} + t_j, \end{cases}$$

where $\boldsymbol{D}_j^{(k)}$, $\boldsymbol{w}_j$, t_j are defined as in (A4). Note that $\boldsymbol{D}_j^{(k)}$ is a diagonal matrix. Thus the derivative of $Q^{(k)}$ at point $\boldsymbol{v}_B$ is

$$Q^{(k)\prime} = \begin{bmatrix} 2\boldsymbol{v}_B^T\boldsymbol{X}_1^{(k)T} + \boldsymbol{y}_1^{(k)T} \\ 2\boldsymbol{v}_B^T\boldsymbol{X}_2^{(k)T} + \boldsymbol{y}_2^{(k)T} \\ \vdots \\ 2\boldsymbol{v}_B^T\boldsymbol{X}_{m+1}^{(k)T} + \boldsymbol{y}_{m+1}^{(k)T} \end{bmatrix} = \begin{bmatrix} 2(\boldsymbol{v}_B^T\boldsymbol{S}^T + \boldsymbol{s}^T)\boldsymbol{D}_1^{(k)} + \boldsymbol{w}_1^{(k)T} \\ 2(\boldsymbol{v}_B^T\boldsymbol{S}^T + \boldsymbol{s}^T)\boldsymbol{D}_2^{(k)} + \boldsymbol{w}_2^{(k)T} \\ \vdots \\ 2(\boldsymbol{v}_B^T\boldsymbol{S}^T + \boldsymbol{s}^T)\boldsymbol{D}_{m+1}^{(k)} + \boldsymbol{w}_{m+1}^{(k)} \end{bmatrix}\boldsymbol{S}. \tag{12}$$

Proposition 2: Define $\varphi^{(k)}_i = 2a^{(k)}_i v_i + b_i$ as the derivative of $g^{(k)}_i$ evaluated at v_i. If $\varphi^{(k)}_i < 0$ for all $i \in I$ and all $\boldsymbol{v}_B \in V_k$, then $Q^{(k)\prime}$ is nonsingular for all $\boldsymbol{v}_B \in V_k$.

Proof: Plugging (4) into (12), we have

$$Q^{(k)\prime} = \boldsymbol{G}^{(k)}\boldsymbol{S},\ \boldsymbol{G}^{(k)} = \begin{bmatrix} 2\boldsymbol{v}^T\boldsymbol{D}_1^{(k)} + \boldsymbol{w}_1^T \\ 2\boldsymbol{v}^T\boldsymbol{D}_2^{(k)} + \boldsymbol{w}_2^T \\ \vdots \\ 2\boldsymbol{v}^T\boldsymbol{D}_{m+1}^{(k)} + \boldsymbol{w}_{m+1}^T \end{bmatrix}. \tag{13}$$

Recall that $\boldsymbol{D}^{(k)}_j \in \mathbb{R}^{(n+m)\times(n+m)}$ and $\boldsymbol{w}_j \in \mathbb{R}^{(n+m)}$ are defined as follows: If the function $g^{(k)}_i(v_i)$ is present in the jth equation of (A3) and v_i corresponds to the lth component of $\boldsymbol{v}$, then the lth diagonal entry of $\boldsymbol{D}^{(k)}_j$ and the lth component of $\boldsymbol{w}_j$ are the coefficients of the quadratic term and the linear term in $g^{(k)}_i(v_i)$, respectively; that is, $\boldsymbol{D}^{(k)}_j(l,l) = \pm a^{(k)}_i$ and $\boldsymbol{w}_j(l) = \pm b_i$, with the same sign in front of $a^{(k)}_i$ and b_i. The other entries of $\boldsymbol{D}^{(k)}_j$ and the other components of $\boldsymbol{w}_j$ are zero.

Using an approach similar to the one we used to show that the matrix $\boldsymbol{\Lambda}$ in the proof of Proposition 1 is nonsingular, by further inspection of (A3) we have

$$\boldsymbol{G}^{(k)} = [\boldsymbol{G}_B^{(k)} \;\; \boldsymbol{G}_N^{(k)}];$$

$$\boldsymbol{G}_B^{(k)} = \begin{bmatrix} \varphi_1^{(k)} & \mp\varphi_{n+1}^{(k)} & 0 & \cdots & \cdots & 0 \\ 0 & \pm\varphi_{n+1}^{(k)} & \mp\varphi_{n+2}^{(k)} & \cdots & \cdots & 0 \\ \vdots & \vdots & \vdots & \ddots & \vdots & \vdots \\ 0 & 0 & 0 & \cdots & \pm\varphi_{n+m-1}^{(k)} & \mp\varphi_{n+m}^{(k)} \\ 0 & 0 & 0 & \cdots & 0 & \pm\varphi_{n+m}^{(k)} \end{bmatrix};$$

$$\boldsymbol{G}_N^{(k)} = \begin{bmatrix} \boldsymbol{\varphi}_0^{(k)T} & \boldsymbol{0}^T & \cdots & \boldsymbol{0}^T & \boldsymbol{0}^T \\ \boldsymbol{0}^T & \boldsymbol{\varphi}_1^{(k)T} & \cdots & \boldsymbol{0}^T & \boldsymbol{0}^T \\ \vdots & \vdots & \ddots & \vdots & \vdots \\ \boldsymbol{0}^T & \boldsymbol{0}^T & \cdots & \boldsymbol{\varphi}_{m-1}^{(k)T} & \boldsymbol{0}^T \\ \boldsymbol{0}^T & \boldsymbol{0}^T & \cdots & \boldsymbol{0}^T & \boldsymbol{\varphi}_m^{(k)T} \end{bmatrix}, \tag{14}$$

where $\boldsymbol{\varphi}^{(k)}_j$ is the vector $[\varphi^{(k)}_{h_j+1}, \ldots, \varphi^{(k)}_{h_{j+1}}]^T$; the sign in front of the entry $\varphi^{(k)}_{n+j}$ ($j = 1, \ldots, m$) in row i, $i = 1, \ldots, m + 1$, is the same as the sign in front of the corresponding quantity $g_{n+j}(v_i)$ in the ith equation in (A3), which is determined according to the rule specified therein. Notice that in the $(j+1)^{\text{st}}$ column of $\boldsymbol{G}_B^{(k)}$, the signs in front of the two adjacent entries $\varphi^{(k)}_{n+j}$ are opposites.

Now utilize form (3c) of the constant matrix $\boldsymbol{C}$, so by (13), $Q^{(k)\prime} = \boldsymbol{G}^{(k)}\boldsymbol{S} = \boldsymbol{F}_B^{(k)} + \boldsymbol{G}_N^{(k)}\boldsymbol{C}$ can be expressed as

$$\begin{bmatrix} \varphi_1^{(k)} + f_{01}^{(k)} & \mp\varphi_{n+1}^{(k)} & 0 & 0 & \cdots & 0 \\ f_{11}^{(k)} & \pm\varphi_{n+1}^{(k)} \pm f_{1,n+1}^{(k)} & \mp\varphi_{n+2}^{(k)} & 0 & \cdots & 0 \\ f_{21}^{(k)} & \pm f_{2,n+1}^{(k)} & \pm\varphi_{n+2}^{(k)} \pm f_{2,n+2}^{(k)} & 0 & \cdots & 0 \\ \vdots & \vdots & \vdots & \vdots & \ddots & \vdots \\ f_{m-1,1}^{(k)} & \pm f_{m-1,n+1}^{(k)} & \pm f_{m-1,n+2}^{(k)} & \pm f_{m-1,n+3}^{(k)} & \cdots & \mp\varphi_{n+m}^{(k)} \\ f_{m,1}^{(k)} & \pm f_{m,n+1}^{(k)} & \pm f_{m,n+2}^{(k)} & \pm f_{m,n+3}^{(k)} & \cdots & \pm\varphi_{n+m}^{(k)} \pm f_{m,n+m}^{(k)} \end{bmatrix}, \tag{15}$$

where we define $f^{(k)}_{jj'} = \boldsymbol{\alpha}_{jj'}^T\boldsymbol{\varphi}^{(k)}_j = \Sigma_{i=h_j+1,\ldots,h_{j+1}} \alpha_{ij'}\varphi^{(k)}_i$. The sign of $f^{(k)}_{jj'}$ is positive if $j' = 1$ or $j' \in I_{\text{in}}$, and negative if $j' \in I_{\text{out}}$. Notice that in (15) we have the following: (i) In each column, the signs in front of the entries $f_{jj'}$ are all the same; (ii) in the $(j + 1)^{\text{st}}$ column, the signs in front of the two adjacent entries $\varphi^{(k)}_{n+j}$ are opposites; (iii) the signs in front of the two terms in every sum $\varphi^{(k)}_{j'} + f^{(k)}_{jj'}$ are the same.

Observations (i)–(iii) are the key to the proof: If $\varphi^{(k)}_i < 0$ for all $i \in I$ and all $\boldsymbol{v}_B \in V_k$, then by adding a positive multiple of row $i + 1$ to row i in (15), starting with $i = m$ and proceeding to $i = 1$, $Q^{(k)\prime}$ can be row reduced to a lower triangular matrix with nonzero diagonal entries. Therefore, if $\varphi^{(k)}_i < 0$ for all $i \in I$ and all $\boldsymbol{v}_B \in V_k$, then $Q^{(k)\prime}$ is nonsingular for all $\boldsymbol{v}_B \in V_k$. ■

Theorem 1: If for every k in $\{1, \ldots, M\}$, $\varphi^{(k)}_i < 0$ for all $i \in I$ and all $\boldsymbol{v}_B \in V_k$, then the system of quadratic equations (10) has at most one solution within V_k for every k in $\{1, \ldots, M\}$.

Proof: If for every k in $\{1, \ldots, M\}$, $\varphi^{(k)}_i < 0$ for all $i \in I$ and all $\boldsymbol{v}_B \in V_k$, then by Proposition 2, $Q^{(k)\prime}$ is nonsingular for all k in $\{1, \ldots, M\}$. And since all V_k are convex by Lemma 3, the result follows from Theorem 3 in [30]. ■

Now we will interpret this sufficient condition, $\varphi^{(k)}_i < 0$, in the context of tunnel ventilation. First, note that by Assumption 1, $b_i < 0$ for all $i \in I$. Then for every segment i that has no local pressure loss or has a fixed flow-independent local pressure-loss coefficient, $\varphi^{(k)}_i = 2a^{(k)}_i v_i + b_i$ is negative since $\xi_i = \zeta_i^0 \geq 0$ for such i. Thus restrictions are needed only for segments i with $\xi_i = \zeta_i^0 + \zeta_i < 0$, and such segments are associated with junctions. Suppose combination k corresponds to the piece $t_j^{(k)}$ for the junction associated with ramp j. Then by (8a) we know that the coefficients $a_i^{(k)}$ for segment $n + j$, and for segment $i = h_j$ (if $j \in I_{\text{in}}$) or segment $i = h_j + 1$ (if $j \in I_{\text{out}}$), are as follows:

$$\begin{cases} a_i^{(k)} = a_i^0 - \dfrac{\alpha_i^{t_j^{(k)}} + \beta_j^{t_j^{(k)}}}{2}; \\ a_{n+j}^{(k)} = a_{n+j}^0 - \dfrac{\alpha_j^{t_j^{(k)}} + \beta_i^{t_j^{(k)}}}{2}, \end{cases} \tag{16}$$

where $a_i^0 = 0.5[q_i L_i A_{vi} / (A_i v_{ti}) - \lambda L_i / d_{ei} - \zeta_i^0]$. Thus for segment $n + j \in \{n + 1, \ldots, n + m\}$, and for segment $i = h_j$ (if $j \in I_{\text{in}}$) or segment $i = h_j + 1$ (if $j \in I_{\text{out}}$), the following hold:

$$\varphi_{n+j}^{(k)} = \frac{V_{t,n+j}A_{v,n+j}}{A_{n+j}v_{t,n+j}}(v_{n+j} - v_{t,n+j}) - \left(\frac{\lambda}{d_{e,n+j}} + \frac{\zeta_j^0}{L_{n+j}} + \alpha_j^{t_j^{(k)}} + \beta_i^{t_j^{(k)}}\right)v_{n+j} - \frac{N_{n+j}A_f K v_f}{A_{n+j}L_j};$$

$$\varphi_i^{(k)} = \frac{V_{ti}A_{vi}}{A_i v_{ti}}(v_i - v_{ti}) - \left(\frac{\lambda}{d_{ei}} + \frac{\zeta_i^0}{L_i} + \alpha_i^{t_j^{(k)}} + \beta_j^{t_j^{(k)}}\right)v_i - \frac{N_i A_f K v_f}{A_i L_i}.$$

This gives us the following corollary of Theorem 1.

Corollary 1: Under Assumption 1, if the following holds for all $j \in \{1, \ldots, m\}$, and for $i = h_j$ (if $j \in I_{\text{in}}$) or $i = h_j + 1$ (if $j \in I_{\text{out}}$), then (10) has at most one solution in V_k for each k in $\{1, \ldots, M\}$:

$$\begin{cases} \alpha_j^{t_j^{(k)}} + \beta_i^{t_j^{(k)}} \geq -\dfrac{\lambda}{d_{e,n+j}} - \dfrac{\zeta_j^0}{L_{n+j}}; \\ \alpha_i^{t_j^{(k)}} + \beta_j^{t_j^{(k)}} \geq -\dfrac{\lambda}{d_{ei}} - \dfrac{\zeta_i^0}{L_i}, \end{cases} \quad \forall k = 1,\ldots,M. \tag{17}$$

The sufficient condition (17) is generally satisfied in real bifurcate tunnels with moderate segment lengths (such as the example in Section V). This is because the friction loss is typically larger than the local pressure losses if the tunnel is not very short. Furthermore, this condition is easily checkable, since $\alpha^{(k)}_i$ and $\beta^{(k)}_i$ are parameters of the PWA function (8a) which are fitted using the techniques presented in Section III, and the other parameters are the given tunnel data. Interestingly, if one wants the inequalities in (17) to hold automatically, they can be imposed in the form of constraints on the PWA function parameters in (8b).

Also, note that if off-ramp segment $n + j$ creates a type-II junction with the mainline, then by the formula given in Table I, we know that the true pressure-loss coefficient at the diverging lateral branch is bounded below by –1; since the outlet loss coefficient is 1, the true value is $\zeta_j \geq 0$. Thus if the PWA function used to approximate the pressure-loss coefficient at the diverging lateral branch is reasonably accurate (i.e., it is also bounded below by –1), then the sufficient condition $\varphi^{(k)}_j < 0$ is also automatically satisfied.

Given this characterization, we can actually solve each of the M systems of quadratic equations relatively efficiently [24], provided that the premise of Theorem 1 holds.

C. Stability analysis

Now we will analyze the stability of the aerodynamic system described by (10), which is a natural extension of our discussion of the steady-state solution (a.k.a. equilibrium point) in the previous subsection. The analysis is based on the fundamental fact that an equilibrium point of a nonlinear system is *asymptotically stable* if and only if all eigenvalues of the Jacobian matrix at that point have negative real parts (e.g., [31]). In our problem setting, let $\boldsymbol{v}_B^*$ be a steady-state solution of (10), let $d\boldsymbol{v}_B/dt = \boldsymbol{F}^{(k)}(\boldsymbol{v}_B)$. Therefore, $\boldsymbol{v}_B^*$ is *asymptotically stable* if and only if the Jacobian matrix $\boldsymbol{F}^{(k)\prime}(\boldsymbol{v}_B^*)$ is Hurwitz (i.e., all its eigenvalues have negative real parts) .

Now we check what this condition implies in our case. By the chain rule, we have the Jacobian matrix at a solution $\boldsymbol{v}_B$ as

$$\boldsymbol{F}^{(k)\prime}(\boldsymbol{v}_B) = \boldsymbol{\Lambda}^{-1} Q^{(k)\prime}(\boldsymbol{v}_B). \tag{18}$$

Proposition 3: If $\varphi^{(k)}_i = 2a^{(k)}_i v_i + b_i < 0$ for all $i \in I$ and all $\boldsymbol{v}_B \in V_k$, then $\boldsymbol{F}^{(k)\prime}(\boldsymbol{v}_B)$ is Hurwitz for all $\boldsymbol{v}_B \in V_k$.

Proof: The idea is to explore the structure of the Jacobian matrix $\boldsymbol{F}^{(k)\prime}(\boldsymbol{v}_B)$. Specifically, utilizing the sign patterns and the proportional lower-entries for the columns in matrices $\boldsymbol{\Lambda}$ and $Q^{(k)\prime}$, we can perform a series of series of matrix decompositions to build the Lyapunov equation. See the Appendix for details. ■

The above proposition involves the most effort in its proof, which directly leads to a main result of our study as below.

Theorem 2: If for every k in $\{1, \ldots, M\}$, $\varphi^{(k)}_i < 0$ for all $i \in I$ and all $\boldsymbol{v}_B \in V_k$, then any steady-state solution to the system of quadratic equations (11) is stable for all k in $\{1, \ldots, M\}$.

Now in analogy to Corollary 1, we have the following corollary regarding the aerodynamic stability of complex tunnels for which the sufficient condition is easily checkable.

Corollary 2: Under Assumption 1, if (17) holds for every $j \in \{1, \ldots, m\}$, and for $i = h_j$ (if $j \in I_{\text{in}}$) or $i = h_j + 1$ (if $j \in I_{\text{out}}$), then any steady-state solution to the system of quadratic equations (11) is stable for all k in $\{1, \ldots, M\}$.

V. A Case Study

For illustration of the proposed methodology, we analyze a hypothetical one-way traffic bifurcate tunnel and focus on the CO concentration limit of 60 mg/m^3. The straight mainline tunnel is divided into $n = 3$ segments and has $m = 2$ literal ramp branches, as shown in Fig. 2, so the basic velocity variables are $\boldsymbol{v}_B = [v_1\ v_4\ v_5]^T$. Each ramp forms a "T-junction" with the mainline tunnel. The on-ramp forms an angle of 60° with the mainline upstream segment (segment 1), while the off-ramp forms an angle of 80° with the mainline downstream segment (segment 5), there is no upper vents.

Other tunnel parameters and the emission data are listed in Table II. The PWA functions are fitted for each of the four local pressure-loss coefficients (calculated according to Table I). Each PWA function has five pieces (i.e., $M_1 = M_2 = 5$), so the total number of piece combinations is $M = 25$. The endpoints of the intervals are chosen to be $\boldsymbol{r}_1 = \boldsymbol{r}_2 = [0.01, 0.2, 0.5, 0.8, 0.9, 0.99]^T$ for the two tunnel junctions. We verify that condition (17) is satisfied for this tunnel, based on the design parameters and the PWA function parameters. We are interested in computing the stable steady-state flow patterns and the resultant CO concentration distributions under various ventilation fan intensities in the tunnel branches.

We discuss two test scenarios. In the first test, the numbers of running jet fan pairs for mainline segments 1, 2, and 3 are

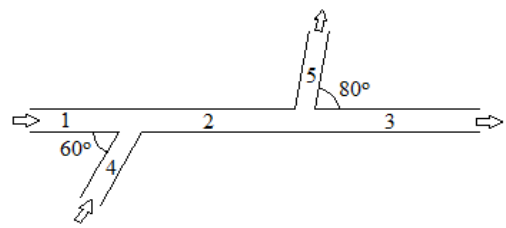

Fig. 2. Example tunnel

fixed at 3, 6, and 6, respectively. We vary the number of running jet fan pairs for each of the on-ramp and off-ramp branches (N_4 and N_5) from 0 to 10. Fig. 3(a) shows the number of steady-state solutions $\boldsymbol{v}_B$ under different combinations of N_4 and N_5. We can see that only one steady-state solution is achieved under most combinations of N_4 and N_5. Under certain combinations of N_4 and N_5, however, there are two steady-state solutions, each from a region defined by V_k for a *distinct* index $k \in \{1, 2, \ldots, 25\}$. In the second test, we look at the steady-state solutions under different fan intensities in two joining flow branches at the first tunnel junction. Specifically, we fix the number of jet fan pairs for mainline segments 2 and 3 at 6, and the number of pairs of jet fans for ramp segment 5 at 3, and we vary the number of jet fan pairs from 0 to 10 for mainline segment 1 and on-ramp segment 4 (N_1 and N_4). As in the previous test, Fig. 3(b) shows that only one steady-state solution is achieved under most combinations of N_1 and N_6. Under some combinations of N_1 and N_6, however, there are also two steady-state solutions $\boldsymbol{v}_B$, each of which corresponds to a *distinct* piece combination $k \in \{1, 2, \ldots, 25\}$. In both tests, every piece combination has at most one steady-state solution, which is

TABLE II Tunnel and Emission Parameters

Notation	Quantity	Value
$L_{1,4,5}$; $L_{2,3}$	Lengths of segments (m)	500; 1000
$A_{1,2,3}$; $A_{4,5}$	Cross-sectional area of segments (m^2)	60; 50
$d_{e1,2,3}$; $d_{e4,5}$	Hydraulic diameter of segments (m)	7.5; 6.67
v_f	Jet speed of jet fans (m/s)	40
A_f	Cross-sectional area of jet fans (m^2)	0.4
K	Pressure-rise coefficient of jet fans	0.88
λ	Tunnel wall friction resistance coefficient	0.02
V_1; $V_{4,5}$	Traffic volume through segments (veh/h)	1000; 500
v_t	Average traffic speed (m/s)	12
$\zeta^0_{1,4}$; $\zeta^0_{3,5}$; ζ^0_2	Flow-independent local loss coefficient	0.6; 1.0; 0
A_v	Equivalent frontal area of vehicles	1.5
$C^{CO}_{amb,\,1,4}$	Ambient CO concentration (mg/m^3)	0.7
$e^{CO}_{1,3}$; e^{CO}_2	CO emission source in mainline (mg/m^3/s)	0.2; 0.3
$e^{CO}_{4,5}$	CO emission source in ramps (mg/m^3/s)	0.1

consistent with Corollary 1. We also note that if N_4 and N_5 are varying (and the other N's fixed), two steady-state solutions are only observed when N_4 equals 8, 18 or 20 (see Fig. 3(a)). But if N_1 and N_4 are varying (and the other N's fixed), two steady-state solutions are observed for various

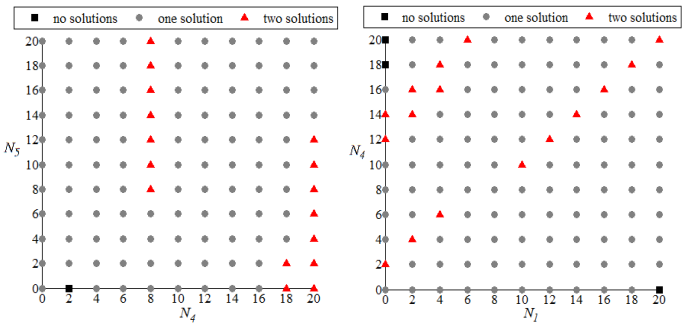

(a) Under different N_4 and N_5 (b) Under different N_1 and N_4

Fig. 3. Number of steady-state solutions of $\boldsymbol{v}_B$

values of N_1 and N_4 with approximately an affine relationship (see Fig. 3(b)). This implies that some pairs of segments may need special investigation.

Table III lists the two steady-state solutions for four fan scenarios, the eigenvalues of the corresponding Jacobian matrices as well as the number of nonattainment tunnel segments (maximum CO concentration > 60 mg/m^3). We verify that all of the solutions are stable, which is consistent with Corollary 2. We also observe that the two steady-state solutions and the CO concentration distributions do not differ very much in the first two scenarios but are quite different in the last two (where the v_i's also differ significantly under either of the two steady-state solutions). This is because in the first two scenarios, the numbers of running fans per unit distance do not differ much over different segments (within a factor of 2), but they change dramatically in the last two scenarios. Hence keeping the numbers of operating fans balanced in different segments is desired for maintain a stable flow in normal operation, and caution is needed in making the fan intensity much higher in some segment than the others during emergencies.

In Fig. 4, we plot the CO concentration distributions in the system under two stable steady-state flow solutions for the fourth fan scenario. The result is generated by evaluating (7) every 100 m in each segment. We can see that the CO concentrations at segments 2~5 are slightly higher under the second solution than those under the first. However, c_1^{CO} is significantly higher under the first solution than that under the second, due to a much lower v_1^* in the first solution, which makes segment 1 become nonattainment segment, and the total number of nonattainment tunnel segments increases by a half (see Table III) compared to that under the second solution. Similar changes are observed for scenario 3. We also notice that under all of these eight stable equilibrium flows, segment 5 is always a nonattainment segment with C_5^{CO} ranging from 86 to 92 mg/m^3, which suggests a need of an upper vents at the downstream part of the tunnel. Therefore, our model analysis offers a rigorous and systematic way of designing effective air quality management strategies for the system.

VI. Conclusions

This study has proposed a steady-state 1-D aerodynamic

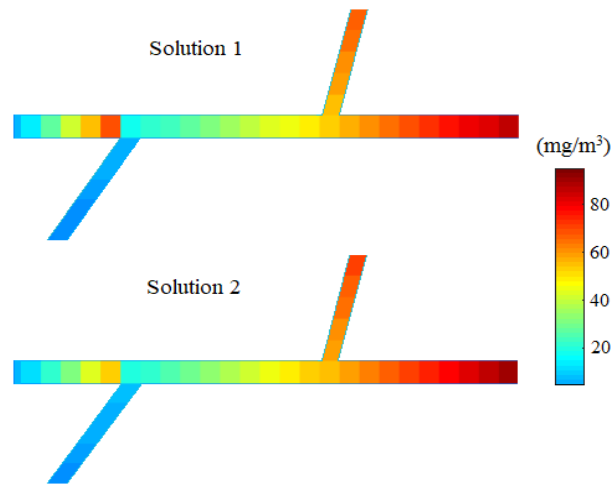

Fig. 4. CO concentration distribution under two steady-state flow solutions (fan scenario #4)

and pollutant dispersion modeling approach for complex urban tunnels based on a system of quadratic equations. In particular, the uniqueness and stability of the equilibrium flows are analyzed. Because local pressure-loss coefficients are flow- dependent, we show that the equilibrium flow pattern and the resultant pollution concentration distribution may not be unique. However, we can bound the number of such equilibrium flows and validate their stability provided that a sufficient condition in terms of the system parameters is satisfied. The results of a case study validate our theoretical derivations and demonstrate the importance of

TABLE III Two Stable Steady-State Solutions

Fan scenario	Steady-state solutions $\boldsymbol{v}_B$ (m/s)			Eigenvalues of $\boldsymbol{F}'(\boldsymbol{v}_B)$ ($\times 10^{-3}$)			#Seg. with $C_i^{CO}(L_i)$ > 60 mg/m^3
	v_1	v_4	v_5	λ_1	λ_2	λ_3	
N_{f1}=12; N_{f4}=12; N_{f5}=6; $N_{f2,3}$=12	4.37	5.44	4.08	-26	-28	-28	2
	4.65	5.02	4.04	-29	-28	-28	2
N_{f4}= 8; N_{f5}=16; N_{f1}= 6; $N_{f2,3}$=12	4.20	5.78	5.52	-34	-26	-25	1
	4.53	5.31	5.48	-34	-26	-28	1
N_{f4}=18; N_{f5}=2; N_{f1}=6; $N_{f2,3}$=12	1.62	8.29	3.17	-21	-29	-25	3
	2.10	7.60	3.09	-30	-22	-26	2
N_{f1}=2; N_{f4} =14; N_{f5}=6; $N_{f2,3}$=12	1.48	8.34	3.73	-20	-27	-27	3
	2.00	7.60	3.65	-22	-29	-27	2

understanding stable equilibrium flows in controlling the CO concentration. With further numerical and experimental analysis, one may also extend the PWA approximation approach to more complicated flow junctions and thus extend the analysis to more general underground networks. Our model offers a convenient tool and theoretical foundation for designing pollutant discharge strategies in complex tunnels, which is crucial for managing underground transport environment during both normal operation and traffic jams.

APPENDIX

A. Proof of Proposition 1

We present the proof in four parts.

First, it is straightforward to show that using the piecewise-affine approximation (8a), we can have a number of quadratic forms similar to $g_i(v_i)$ whose parameters depend on which "piece" the flow ratio lies in for each junction.

Specifically, based on (6) and (8a), we can define a quadratic function $g_i^{(k)}(v_i) = a_i^{(k)}v_i^2 + b_iv_i + c_i$ for each combination $k = 1, \ldots, M$ of pieces of the approximation functions for the loss coefficients at the tunnel junctions. By construction, each of the approximation functions is a function of the reciprocal of the squared flow ratio, so the coefficients b_i and c_i are independent of k for all $i \in I$ and are the same as defined in (4). For each segment $i \in \{1, \ldots, n\} \backslash \{I_{in}^{main} \cup I_{out}^{main}\}$, the local loss coefficient ζ_i is constant, so $a_i^{(k)} = a_i$ is the same as defined in (4). Suppose combination k corresponds to piece t_j for the junction associated with ramp segment $n + j$ (j=1, …, m). Then the coefficients $a_i^{(k)}$ for those segments ($n + j$ for all j, and for $i = h_j$ if $j \in I_{in}$ and for $i = h_j + 1$ if $j \in I_{out}$) with flow-dependent ζ are

$$\begin{cases} a_i = a_i^0 - \alpha_i^{(t_j)}/2 - \beta_j^{(t_j)}/2; \\ a_{n+j} = a_{n+j}^0 - \alpha_j^{(t_j)}/2 - \beta_i^{(t_j)}/2, \end{cases} \tag{A1}$$

where $a_i^0 = 0.5[q_iL_iA_{vi}/(A_iv_{ti}) - \lambda L_i/d_{ei} - \zeta_i^0]$.

Second, we eliminate the boundary pressure variables in (6) by the following steps:

(i) For $i = h_j$ with $j - n \in I_{in}$, we have $p_i = g_j(v_j) - L_jdv_j/dt$, and for $i = h_j$ with $j \in I_{out}$, we have $p_i = L_jdv_j/dt - g_j(v_j)$. This is based on the last two equations in (6), which encode the "*pressure balance*" condition at the tunnel junctions.

(ii) For all pairs of adjacent ramps j, j' ($1 \le j, j' \le m$, $j' = j + 1$), do the following: If there is at least one segment between segments h_j and $h_{j'}$, then combining the first equation in (6) over $\{i: h_{j'} < i \le h_{j'}\}$, we have

$$p_{h_j} - p_{h_{j'}} + \sum_{i=h_j+1}^{h_{j'}} g_i(v_i) = \sum_{i=h_j+1}^{h_{j'}} L_i \frac{dv_i}{dt}, \tag{A2a}$$

(iii) Using a similar technique as in (ii), sum the first equation in (6) over $\{i: 1 \le i \le h_1\}$ and over $\{i: h_m < i \le n\}$, which gives

$$-p_{h_1} + \sum_{i=1}^{h_1} g_i(v_i) = \sum_{i=1}^{h_1} L_i \frac{dv_i}{dt};\ p_{h_m} + \sum_{i=h_m+1}^{n} g_i(v_i) = \sum_{i=h_m+1}^{n} L_i \frac{dv_i}{dt}. \tag{A2b}$$

(iv) Use the expressions in (i) to eliminate the boundary pressure terms in (A2a) and (A2b).

After performing steps (i)–(iv) above, the boundary pressure variables of the $n - 1$ segments are all eliminated, so (6) becomes a system of $(n + m) - (n - 1) = m + 1$ equations in $n + m$ air-velocity variables:

$$\begin{cases} L_1\dot{v}_1 \pm L_{n+1}\dot{v}_{n+1} + \sum_{i=2}^{h_1} L_i\dot{v}_i = g_1^{(k)}(v_1) \pm g_{n+1}^{(k)}(v_{n+1}) + \sum_{i=2}^{h_1} g_i^{(k)}(v_i); \\ \pm L_{n+1}\dot{v}_{n+1} \pm L_{n+2}\dot{v}_{n+2} + \sum_{i=h_1+1}^{h_2} L_i\dot{v}_i = \pm g_{n+1}^{(k)}(v_{n+1}) \pm g_{n+2}^{(k)}(v_{n+2}) + \sum_{i=h_1+1}^{h_2} g_i^{(k)}(v_i); \\ \qquad \vdots \\ \pm L_{n+m}\dot{v}_{n+m} + \sum_{i=h_m+1}^{n} L_i\dot{v}_i = \pm g_{n+m}^{(k)}(v_{n+m}) + \sum_{i=h_m+1}^{n} g_i^{(k)}(v_i), \end{cases} \tag{A3}$$

where $\dot{x}$ denotes dx/dt. In the last equation in (A3), the sign in front of $g_{n+m}(v_{n+m})$ is positive if $m \in I_{in}$ and negative if $m \in I_{out}$. In the other two equations, the sign in front of the term $g_{n+j}(v_{n+j})$ that is closer to the summation is negative if $j \in I_{in}$ and positive if $j \in I_{out}$; the sign in front of the other term $g_{n+j}(v_{n+j})$ is positive if $j \in I_{in}$ and negative otherwise. The sign in front of each term Ln+jdvn+j/dt is the same as that of the sign in front of the corresponding term $g_{n+j}(v_{n+j})$.

Third, we express (A3) in terms of only the basic velocity variables $\boldsymbol{v}_B$. Define $\boldsymbol{L} = [\boldsymbol{L}_B^T,\ \boldsymbol{L}_N^T]^T$, where $\boldsymbol{L}_B$ and $\boldsymbol{L}_N$ partition $\{L_1, \ldots, L_{m+n}\}$ in accordance with the partition of $\{v_1, \ldots, v_{m+n}\}$ by v_B and v_N. Then by (4), the jth equation in (A3) can be expressed as

$$\begin{aligned} &\boldsymbol{L}^T\boldsymbol{T}_j\boldsymbol{S}\dot{\boldsymbol{v}}_B \\ &= (\boldsymbol{S}\boldsymbol{v}_B + \boldsymbol{s})^T\boldsymbol{D}_j^{(k)}(\boldsymbol{S}\boldsymbol{v}_B + \boldsymbol{s}) + \boldsymbol{w}_j^T(\boldsymbol{S}\boldsymbol{v}_B + \boldsymbol{s}) + t_j, \end{aligned} \tag{A4}$$

where $\boldsymbol{T}_j \in \mathbb{R}^{(n+m)\times(n+m)}$ and $\boldsymbol{D}^{(k)}_j \in \mathbb{R}^{(n+m)\times(n+m)}$ are both diagonal matrices, $\boldsymbol{w}_j \in \mathbb{R}^{(n+m)}$, and $t_j \in \mathbb{R}$. In the jth equation of (A3), if $g^{(k)}_i(v_i)$ is present and v_i corresponds to the lth component of vector $\boldsymbol{v}$, then the lth diagonal entry of $\boldsymbol{T}_j$ is ±1, the lth diagonal entry of $\boldsymbol{D}^{(k)}_j$ is $\pm a^{(k)}_i$, and the lth component of $\boldsymbol{w}_j$ is $\pm b_i$ (the rule of setting the signs is the same as that specified for (A3)). The other entries in $\boldsymbol{T}_j$, $\boldsymbol{D}^{(k)}_j$ and $\boldsymbol{w}_j$ are zero, and t_j is the sum of the other constant terms (i.e., the ± c_i's). Note that unlike $\boldsymbol{D}^{(k)}_j$, $\boldsymbol{w}_j$ and t_j do not have a superscript "(k)," since the piecewise approximation does not affect the coefficients b_i, c_i.

Now if we define (for j = 1, …, m + 1)

$$\begin{cases} \boldsymbol{X}_j^{(k)} = \boldsymbol{S}^T\boldsymbol{D}_j^{(k)}\boldsymbol{S}; \\ \boldsymbol{y}_j^{(k)} = 2\boldsymbol{S}^T\boldsymbol{D}_j^{(k)}\boldsymbol{s} + \boldsymbol{S}^T\boldsymbol{w}_j; \\ z_j^{(k)} = \boldsymbol{s}^T\boldsymbol{D}_j^{(k)}\boldsymbol{s} + \boldsymbol{w}_j^T\boldsymbol{s} + t_j, \end{cases} \tag{A5}$$

then the jth equation in (A3) is equivalent to

$$\boldsymbol{L}^T\boldsymbol{T}_j\boldsymbol{C}\dot{\boldsymbol{v}}_B = \boldsymbol{v}_B^T\boldsymbol{X}_j^{(k)}\boldsymbol{v}_B + \boldsymbol{y}_j^{(k)T}\boldsymbol{v}_B + z_j^{(k)}. \tag{A6}$$

Note that $\boldsymbol{X}^{(k)}_j$ is symmetric, since

$$\begin{aligned} \boldsymbol{X}_j^{(k)}(s,t) &= \sum_h \boldsymbol{S}^T(s,h)\boldsymbol{D}_j^{(k)}(h,h)\boldsymbol{S}(h,t) \\ &= \sum_h \boldsymbol{S}^T(t,h)\boldsymbol{D}_j^{(k)}(h,h)\boldsymbol{S}(h,s) \\ &= \boldsymbol{X}_j^{(k)}(t,s). \end{aligned}$$

Finally, we form the constant matrix $\boldsymbol{\Lambda} \in \mathbb{R}^{(m+1)\times(m+1)}$ and show that it has full rank. Since $\boldsymbol{L} = [\boldsymbol{L}_B^T,\ \boldsymbol{L}_N^T]^T$, from the expression for $\boldsymbol{C}$ and (A6) we have

$$\begin{aligned} &\boldsymbol{\Lambda} = \begin{bmatrix} \boldsymbol{\Gamma}_B & \boldsymbol{\Gamma}_N \end{bmatrix} \begin{bmatrix} \boldsymbol{I} \\ -\boldsymbol{C} \end{bmatrix} = \boldsymbol{\Gamma}_B - \boldsymbol{\Gamma}_N\boldsymbol{C}; \\ &\boldsymbol{\Gamma}_B = \begin{bmatrix} \boldsymbol{L}_B^T\boldsymbol{T}_1 \\ \vdots \\ \boldsymbol{L}_B^T\boldsymbol{T}_{m+1} \end{bmatrix},\ \boldsymbol{\Gamma}_N = \begin{bmatrix} \boldsymbol{L}_N^T\boldsymbol{T}_1 \\ \vdots \\ \boldsymbol{L}_N^T\boldsymbol{T}_{m+1} \end{bmatrix}. \end{aligned} \tag{A7a}$$

By further inspection of (A3), $\boldsymbol{\Gamma}_B$ and $\boldsymbol{\Gamma}_N$ can be expressed as:

$$\boldsymbol{\Gamma}_B = \begin{bmatrix} L_1 & \mp L_{n+1} & 0 & \cdots & \cdots & 0 \\ 0 & \pm L_{n+1} & \mp L_{n+2} & \cdots & \cdots & 0 \\ \vdots & \vdots & \vdots & \ddots & \vdots & \vdots \\ 0 & 0 & 0 & \cdots & \pm L_{n+m-1} & \mp L_{n+m} \\ 0 & 0 & 0 & \cdots & 0 & \pm L_{n+m} \end{bmatrix}; \quad \text{(A7b)}$$

$$\boldsymbol{\Gamma}_N = \begin{bmatrix} \boldsymbol{L}_0^T & \boldsymbol{0}^T & \cdots & \boldsymbol{0}^T & \boldsymbol{0}^T \\ \boldsymbol{0}^T & \boldsymbol{L}_1^T & \cdots & \boldsymbol{0}^T & \boldsymbol{0}^T \\ \vdots & \vdots & \ddots & \vdots & \vdots \\ \boldsymbol{0}^T & \boldsymbol{0}^T & \cdots & \boldsymbol{L}_{m-1}^T & \boldsymbol{0}^T \\ \boldsymbol{0}^T & \boldsymbol{0}^T & \cdots & \boldsymbol{0}^T & \boldsymbol{L}_m^T \end{bmatrix},$$

where $\boldsymbol{L}_j$ is the vector $[L_{h_j+1}, \ldots, L_{h_{j+1}}]^T$ (let $h_0 = 1$ and $h_{m+1} = n$). For every i in $\{1, \ldots, m + 1\}$, the sign in front of the entry L_{n+j} ($j = 1, \ldots, m$) in row $i$is the same as the sign in front of the corresponding term L_{n+j} in the ith equation in (A3). Notice that in the $(j + 1)^{\text{st}}$ column of $\boldsymbol{\Gamma}_B$, the signs in front of the two adjacent terms L_{n+j} are opposites.

Let $l_{jj'} = \boldsymbol{\alpha}_{jj'}{}^T\boldsymbol{L}_j = \Sigma_{i=h_j+1\ldots h_{j+1}}\alpha_{ij'}L_i$. Then by (A7a) and the expression for $\boldsymbol{C}$ given in (3c), $\boldsymbol{\Lambda}$ can be expressed as

$$\begin{bmatrix} l_{01}+L_1 & \mp L_{n+1} & 0 & \cdots & 0 \\ l_{11} & \pm l_{1,n+1} \pm L_{1,n+1} & \mp L_{n+2} & \cdots & 0 \\ l_{21} & \pm l_{2,n+1} & \pm l_{2,n+2} \pm L_{n+2} & \ddots & 0 \\ \vdots & \vdots & \vdots & \vdots & \vdots \\ l_{m-1,1} & \pm l_{m-1,n+1} & \pm l_{m-1,n+2} & \cdots & \mp L_{n+m} \\ l_{m,1} & \pm l_{m,n+1} & \pm l_{m,n+2} & \cdots & \pm l_{m,n+m} \pm L_{n+m} \end{bmatrix}, \quad \text{(A8)}$$

where the sign in front of $l_{jj'}$ is positive if $j' = 1$ or $j' \in I_{\text{in}}$, and negative if $j' \in I_{\text{out}}$. Notice that in (A8) the following hold: (i) In each column, the signs in front of the entries $l_{jj'}$ are all the same; (ii) in the $(j+1)^{\text{st}}$ column, the signs in front of the two adjacent entries L_{n+j} are opposites; (iii) the signs in front of the two terms in every sum $L_{j'} + l_{jj'}$ are the same.

From (i)–(iii), we obtain the following: Since $L_i > 0$ for all $i \in I$, by adding a proper positive multiple of row $i + 1$ to row i in (A8), starting with $i = m$ and proceeding to $i = 1$, $\boldsymbol{\Lambda}$ can be row reduced to a lower triangular matrix whose diagonal entries are all nonzero, so $\boldsymbol{\Lambda}$ is nonsingular. ■

B. Proof of Proposition 3

Our idea is to prove that a matrix similar to $\boldsymbol{F}^{(k)\prime}$ (i.e., has the same spectrum with $\boldsymbol{F}^{(k)\prime}$) is Hurwitz. To show this, we utilize the structure of $\boldsymbol{F}^{(k)\prime} = \boldsymbol{\Lambda}^{-1}Q^{(k)\prime}$ and decompose it into several special matrices. We present this in five parts.

First, note that the two matrices $\boldsymbol{\Lambda}$ and Q' have the same sign pattern: the first column is positive; and for each column 2 to $m + 1$, the first nonzero entry has the opposite sign with the rest of the entries in the same column. The column indices $\{2, 3, \ldots, m + 1\}$ are partitioned into two known sets: J_1 and J_2, the first nonzero entry of column j is positive if $j \in J_1$, and is negative if $j \in J_2$. For example, if $m = 3$, $J_1 = \{2, 4\}$ and $J_2 = \{3\}$, then the sign pattern of the two matrices is

$$\begin{bmatrix} + & + & 0 & 0 \\ + & - & - & 0 \\ + & - & + & + \\ + & - & + & - \end{bmatrix}.$$

For convenience, we define $\boldsymbol{Q} = -Q'$ (the superscript "(k)" is omitted through the proof for simplicity). We factor $\boldsymbol{\Lambda}$ and $\boldsymbol{Q}$ into products of two triangular matrices and a diagonal matrix. By the definition of $f_{jj'}$ in (15) and $l_{jj'}$ in (A8), we know $f_{jj'}/f_{jj''} = l_{jj'}/l_{jj''} = A_{j'}/A_{j''}$. Then if we define $\mu_j = A_{n+j}/A_1$ ($j = 1, \ldots, m$), we can write $\boldsymbol{\Lambda}$ and $\boldsymbol{Q}$ as

$$\boldsymbol{\Lambda} = \begin{bmatrix} l_{01}+L_1 & \mp L_1 & 0 & \cdots & 0 \\ l_{11} & \pm\mu_1 l_{11} \pm L_1 & \mp L_2 & \cdots & 0 \\ l_{21} & \pm\mu_1 l_{21} & \pm\mu_2 l_{21} \pm L_2 & \ddots & 0 \\ \vdots & \vdots & \vdots & \vdots & \vdots \\ l_{m-1,1} & \pm\mu_1 l_{m-1,1} & \pm\mu_2 l_{m-1,1} & \cdots & \mp L_m \\ l_{m,1} & \pm\mu_1 l_{m,1} & \pm\mu_2 l_{m,1} & \cdots & \pm\mu_m l_{m,1} \pm L_m \end{bmatrix}, \quad \text{(A9a)}$$

$$\boldsymbol{Q} = \begin{bmatrix} -f_{01}-\varphi_1 & \pm\varphi_1 & 0 & \cdots & 0 \\ -f_{11} & \mp\mu_1 f_{11} \mp\varphi_1 & \pm\varphi_2 & \cdots & 0 \\ -f_{21} & \mp\mu_1 f_{21} & \mp\mu_2 f_{21} \mp\varphi_2 & \cdots & 0 \\ \vdots & \vdots & \vdots & \ddots & \vdots \\ -f_{m-1,1} & \mp\mu_1 f_{m-1,1} & \mp\mu_2 f_{m-1,1} & \cdots & \pm\varphi_m \\ -f_{m,1} & \mp\mu_1 f_{m,1} & \mp\mu_2 f_{m,1} & \cdots & \mp\mu_m f_{m,1} \mp\varphi_m \end{bmatrix}. \quad \text{(A9b)}$$

By the proof of *Proposition 1* and *2*, we can write

$$\boldsymbol{U}_1\boldsymbol{\Lambda} = \boldsymbol{L}_1\boldsymbol{D}_0, \quad \boldsymbol{U}_2\boldsymbol{Q} = \boldsymbol{L}_2\boldsymbol{D}_0, \quad \text{(A10a)}$$

equivalently,

$$\boldsymbol{\Lambda} = \boldsymbol{U}_1^{-1}\boldsymbol{L}_1\boldsymbol{D}_0, \quad \boldsymbol{Q} = \boldsymbol{U}_2^{-1}\boldsymbol{L}_2\boldsymbol{D}_0, \quad \text{(A10b)}$$

where $\boldsymbol{D}_0$ is a diagonal matrix whose diagonal entries are $1, \pm\mu_1, \pm\mu_2, \ldots, \pm\mu_m$ (the signs of each μ_j is positive if $j \in I_{\text{in}}$ and negative $j \in I_{\text{out}}$). $\boldsymbol{U}_1$ and $\boldsymbol{U}_2$ are upper triangular matrices; $\boldsymbol{L}_1$ and $\boldsymbol{L}_2$ are lower triangular matrices. These triangular matrices are

$$\boldsymbol{L}_1 = \begin{bmatrix} \tilde{l}_0 & 0 & \cdots & 0 & 0 \\ \tilde{l}_1 & \tilde{l}_1+\tilde{L}_1 & \cdots & 0 & 0 \\ \vdots & \vdots & \ddots & \vdots & \vdots \\ \tilde{l}_{m-1} & \tilde{l}_{m-1} & \cdots & \tilde{l}_{m-1}+\tilde{L}_{m-1} & 0 \\ \tilde{l}_m & \tilde{l}_m & \cdots & \tilde{l}_m & \tilde{l}_m+\tilde{L}_m \end{bmatrix}, \quad \text{(A11a)}$$

$$\boldsymbol{L}_2 = -\begin{bmatrix} \tilde{f}_0 & 0 & \cdots & 0 & 0 \\ \tilde{f}_1 & \tilde{f}_1+\tilde{\varphi}_1 & \cdots & 0 & 0 \\ \vdots & \vdots & \ddots & \vdots & \vdots \\ \tilde{f}_{m-1} & \tilde{f}_{m-1} & \cdots & \tilde{f}_{m-1}+\tilde{\varphi}_{m-1} & 0 \\ \tilde{f}_m & \tilde{f}_m & \cdots & \tilde{f}_m & \tilde{f}_m+\tilde{\varphi}_m \end{bmatrix}, \quad \text{(A11b)}$$

$$\boldsymbol{U}_1 = \begin{bmatrix} 1 & \gamma_1 & \gamma_1\gamma_2 & \cdots & \prod_{i=1}^{m-1}\gamma_i & \prod_{i=1}^{m}\gamma_i \\ 0 & 1 & \gamma_2 & \cdots & \prod_{i=2}^{m-1}\gamma_i & \prod_{i=2}^{m}\gamma_i \\ \vdots & \vdots & \vdots & \ddots & \vdots & \vdots \\ 0 & 0 & 0 & \cdots & 1 & \gamma_m \\ 0 & 0 & 0 & \cdots & 0 & 1 \end{bmatrix}, \quad \text{(A11c)}$$

$$\boldsymbol{U}_2 = \begin{bmatrix} 1 & \tau_1 & \tau_1\tau_2 & \cdots & \prod_{i=1}^{m-1}\tau_i & \prod_{i=1}^{m}\tau_i \\ 0 & 1 & \tau_2 & \cdots & \prod_{i=2}^{m-1}\tau_i & \prod_{i=2}^{m}\tau_i \\ \vdots & \vdots & \vdots & \ddots & \vdots & \vdots \\ 0 & 0 & 0 & \cdots & 1 & \tau_m \\ 0 & 0 & 0 & \cdots & 0 & 1 \end{bmatrix}, \quad \text{(A11d)}$$

where

$$\tilde{L}_i = L_{n+i}/\mu_i; \quad \tilde{\varphi}_i = \varphi_{n+i}/\mu_i, \quad i = 1,\ldots, m;$$
$$\gamma_i = \tilde{L}_i/(\tilde{l}_i + \tilde{L}_i); \quad \tau_i = \tilde{\varphi}_i/(\tilde{f}_i + \tilde{\varphi}_i), \quad i = 1,\ldots, m;$$
$$\tilde{l}_i = \begin{cases} l_{i,1} + L_1 + (1-\gamma_{i+1})\tilde{l}_{i+1}, & \text{if } i = 0; \\ l_{i,1} + (1-\gamma_{i+1})\tilde{l}_{i+1}, & \text{if } i = 1,\ldots, m-1; \\ l_{i,1}, & \text{if } i = m; \end{cases} \tag{A11e}$$
$$\tilde{f}_i = \begin{cases} f_{i,1} + \varphi_1 + (1-\tau_{i+1})\tilde{f}_{i+1}, & \text{if } i = 0; \\ f_{i,1} + (1-\tau_{i+1})\tilde{f}_{i+1}, & \text{if } i = 1,\ldots, m-1; \\ f_{i,1}, & \text{if } i = m. \end{cases}$$

Note that all the nonzero entries of $\boldsymbol{L}_1$, $\boldsymbol{U}_1$, $\boldsymbol{U}_2$ are positive. Furthermore, if $\varphi_i < 0$ for all $i \in I$ (the sufficient condition to be proved), all the nonzero entries of $\boldsymbol{L}_2$ are also positive.

Second, we form a matrix that is similar to $-\boldsymbol{F}'$ and can be written as a product of an upper and a lower triangular matrices. By (18) and (A10b), we can express $-\boldsymbol{F}'$ as

$$-\boldsymbol{F}' = \boldsymbol{\Lambda}^{-1}\boldsymbol{Q} = \boldsymbol{D}_0^{-1}\boldsymbol{L}_1^{-1}\boldsymbol{U}_1\boldsymbol{U}_2^{-1}\boldsymbol{L}_2\boldsymbol{D}_0. \tag{A12}$$

Now let $\boldsymbol{E} = \boldsymbol{L}_1\boldsymbol{D}_0$ (so $\boldsymbol{E}$ is nonsingular), $\boldsymbol{U} = \boldsymbol{U}_1\boldsymbol{U}_2^{-1}$ (so $\boldsymbol{U}$ is also an upper triangular matrix), $\boldsymbol{L} = \boldsymbol{L}_2\boldsymbol{L}_1^{-1}$ (so $\boldsymbol{L}$ is also a lower triangular matrix), using (A12) we can define

$$\boldsymbol{G} = \boldsymbol{E}\boldsymbol{F}'\boldsymbol{E}^{-1} = \boldsymbol{L}_1\boldsymbol{D}_0\boldsymbol{D}_0^{-1}\boldsymbol{L}_1^{-1}\boldsymbol{U}_1\boldsymbol{U}_2^{-1}\boldsymbol{L}_2\boldsymbol{D}_0\boldsymbol{D}_0^{-1}\boldsymbol{L}_1^{-1} = \boldsymbol{U}\boldsymbol{L}. \tag{A13}$$

Hence $\boldsymbol{G}$ has the same eigenvalues as $-\boldsymbol{F}'$, so it is sufficient to show that all the eigenvalues of $\boldsymbol{G}$ have positive real parts.

Third, we compute $\boldsymbol{U}$ explicitly. By the form of $\boldsymbol{U}_2$ given in (A11d), it is not hard to check that

$$\boldsymbol{U}_2^{-1} = \begin{bmatrix} 1 & -\tau_1 & \cdots & 0 & 0 & 0 \\ \vdots & \vdots & \ddots & \vdots & \vdots & \vdots \\ 0 & 0 & \cdots & 1 & -\tau_{m-1} & 0 \\ 0 & 0 & \cdots & 0 & 1 & -\tau_m \\ 0 & 0 & \cdots & 0 & 0 & 1 \end{bmatrix}. \tag{A14}$$

Combining (A11c) and (A14) gives us the expression for $\boldsymbol{U} = \boldsymbol{U}_1\boldsymbol{U}_2^{-1}$ as

$$\begin{bmatrix} 1 & \gamma_1-\tau_1 & (\gamma_2-\tau_2)\gamma_1 & \cdots & (\gamma_{m-1}-\tau_{m-1})\prod_{i=1}^{m-2}\gamma_i & (\gamma_m-\tau_m)\prod_{i=1}^{m-1}\gamma_i \\ 0 & 1 & \gamma_2-\tau_2 & \cdots & (\gamma_2-\tau_2)\prod_{i=2}^{m-2}\gamma_i & (\gamma_2-\tau_2)\prod_{i=2}^{m-1}\gamma_i \\ \vdots & \vdots & \vdots & \ddots & \vdots & \vdots \\ 0 & 0 & 0 & \cdots & \gamma_{m-1}-\tau_{m-1} & (\gamma_m-\tau_m)\gamma_{m-1} \\ 0 & 0 & 0 & \cdots & 1 & \gamma_m-\tau_m \\ 0 & 0 & 0 & \cdots & 0 & 1 \end{bmatrix}. \tag{A15}$$

Fourth, we scale columns of $\boldsymbol{L}$ properly to express it in neat form. It can be verified from (A11a) that if we define a diagonal matrix $\boldsymbol{D}_1$ that has the same diagonal entries as $\boldsymbol{L}_1$, then we can express $\boldsymbol{L}_1$ as $\boldsymbol{L}_1 = \boldsymbol{D}_1\underline{\boldsymbol{L}}_1$, where

$$\underline{\boldsymbol{L}}_1 = \begin{bmatrix} 1 & 0 & \cdots & 0 & 0 \\ 1-\gamma_1 & 1 & \cdots & 0 & 0 \\ \vdots & \vdots & \ddots & \vdots & \vdots \\ 1-\gamma_{m-1} & 1-\gamma_{m-1} & \cdots & 1 & 0 \\ 1-\gamma_m & 1-\gamma_m & \cdots & 1-\gamma_m & 1 \end{bmatrix}. \tag{A16}$$

The below-diagonal entries in $\underline{\boldsymbol{L}}_1$ take the form above due to a key relation and the definition of γ_i in (A11e)

$$\frac{\tilde{l}_i}{\tilde{l}_i + \tilde{L}_i} = 1 - \frac{\tilde{L}_i}{\tilde{l}_i + \tilde{L}_i} = 1 - \gamma_i.$$

And since $\boldsymbol{L}_1 = \boldsymbol{D}_1\underline{\boldsymbol{L}}_1$, we have

$$\boldsymbol{L}_1^{-1} = \underline{\boldsymbol{L}}_1^{-1}\boldsymbol{D}_1^{-1}. \tag{A17}$$

By (A16) we know that entries $\underline{\boldsymbol{L}}_1^{-1}(i, i) = 1$ and $\underline{\boldsymbol{L}}_1^{-1}(i, j) = 0$ ($i < j$). And since in each row of $\underline{\boldsymbol{L}}_1$, all the nonzero off-diagonal entries are the same, it is easy to see that the rest of the entries $\underline{\boldsymbol{L}}_1^{-1}(i, j)$ (where $i > j$) can be computed recursively from $i = 2$ to $i = m$ for each column $j = 1, \ldots, m$ as below

$$\underline{\boldsymbol{L}}_1^{-1}(i, j) = -\underline{\boldsymbol{L}}_1(i, j)\sum_{i'=j}^{i-1}\underline{\boldsymbol{L}}_1^{-1}(i', j).$$

This recursion yields a nice form of $\underline{\boldsymbol{L}}_1^{-1}$ (which can be verified by induction on rows)

$$\underline{\boldsymbol{L}}_1^{-1} = \begin{bmatrix} 1 & 0 & \cdots & 0 & 0 \\ \gamma_1 - 1 & 1 & \cdots & 0 & 0 \\ (\gamma_2-1)\gamma_1 & \gamma_2 - 1 & \cdots & 0 & 0 \\ \vdots & \vdots & \ddots & \vdots & \vdots \\ (\gamma_{m-1}-1)\prod_{i=1}^{m-2}\gamma_i & (\gamma_{m-1}-1)\prod_{i=2}^{m-2}\gamma_i & \cdots & 1 & 0 \\ (\gamma_m-1)\prod_{i=1}^{m-1}\gamma_i & (\gamma_m-1)\prod_{i=2}^{m-1}\gamma_i & \cdots & \gamma_m - 1 & 1 \end{bmatrix}, \tag{A18}$$

Then using (A11b) and (A18), we have $\boldsymbol{L}_2\underline{\boldsymbol{L}}_1^{-1}$ equal to (where we denote $\underline{\gamma}_i = \gamma_i - 1$)

$$-\begin{bmatrix} \tilde{f}_0 & 0 & \cdots & 0 & 0 \\ \gamma_1\tilde{f}_1 + \underline{\gamma}_1\tilde{\varphi}_1 & \tilde{f}_1 + \tilde{\varphi}_1 & \cdots & 0 & 0 \\ \gamma_1(\gamma_2\tilde{f}_1 + \underline{\gamma}_2\tilde{\varphi}_1) & \gamma_2\tilde{f}_2 + \underline{\gamma}_2\tilde{\varphi}_2 & \cdots & 0 & 0 \\ \vdots & \vdots & \ddots & \vdots & \vdots \\ (\gamma_{m-1}\tilde{f}_{m-1} + \underline{\gamma}_{m-1}\tilde{\varphi}_{m-1})\prod_{i=1}^{m-2}\gamma_i & (\gamma_{m-1}\tilde{f}_{m-1} + \underline{\gamma}_{m-1}\tilde{\varphi}_{m-1})\prod_{i=2}^{m-2}\gamma_i & \cdots & \tilde{f}_{m-1} + \tilde{\varphi}_{m-1} & 0 \\ (\gamma_m\tilde{f}_m + \underline{\gamma}_m\tilde{\varphi}_m)\prod_{i=1}^{m-1}\gamma_i & (\gamma_m\tilde{f}_m + \underline{\gamma}_m\tilde{\varphi}_m)\prod_{i=2}^{m-1}\gamma_i & \cdots & \gamma_m\tilde{f}_m + \underline{\gamma}_m\tilde{\varphi}_m & \tilde{f}_m + \tilde{\varphi}_m \end{bmatrix}.$$

Here comes a key step: we define a diagonal matrix $\boldsymbol{D}_2$ that has the same diagonal entries as $\boldsymbol{L}_2$ (so $\boldsymbol{D}_2$ is positive), and we define the following auxiliary variables

$$\omega_0 = \frac{\tilde{f}_1 + \tilde{\varphi}_1}{\tilde{f}_0}; \quad \omega_i = \frac{\tilde{f}_{i+1} + \tilde{\varphi}_{i+1}}{\tilde{f}_i + \tilde{\varphi}_i}, \quad i = 1,\ldots, m, \tag{A19}$$

then we define $\bar{\boldsymbol{L}} = \boldsymbol{L}_2\underline{\boldsymbol{L}}_1^{-1}\boldsymbol{D}_2^{-1}$, which can be expressed as

$$\begin{bmatrix} 1 & 0 & \cdots & 0 & 0 \\ (\gamma_1-\tau_1)\omega_1 & 1 & \cdots & 0 & 0 \\ (\gamma_2-\tau_2)\gamma_1\omega_1\omega_2 & (\gamma_2-\tau_2)\omega_2 & \cdots & 0 & 0 \\ \vdots & \vdots & \ddots & \vdots & \vdots \\ (\gamma_{m-1}-\tau_{m-1})\prod_{i=1}^{m-2}\gamma_i\prod_{i=1}^{m-1}\omega_i & (\gamma_{m-1}-\tau_{m-1})\prod_{i=2}^{m-2}\gamma_i\prod_{i=2}^{m-1}\omega_i & \cdots & 1 & 0 \\ (\gamma_m-\tau_m)\prod_{i=1}^{m-1}\gamma_i\prod_{i=1}^{m}\omega_i & (\gamma_m-\tau_m)\prod_{i=2}^{m-1}\gamma_i\prod_{i=2}^{m}\omega_i & \cdots & (\gamma_m-\tau_m)\omega_m & 1 \end{bmatrix}. \tag{A20}$$

By (A17), $\boldsymbol{L} = \boldsymbol{L}_2\boldsymbol{L}_1^{-1} = \boldsymbol{L}_2\underline{\boldsymbol{L}}_1^{-1}\boldsymbol{D}_1^{-1}$, so

$$\begin{aligned} \boldsymbol{G} &= \boldsymbol{U}\boldsymbol{L}_2\underline{\boldsymbol{L}}_1^{-1}\boldsymbol{D}_1^{-1} \\ &= \boldsymbol{U}\boldsymbol{L}_2\underline{\boldsymbol{L}}_1^{-1}\boldsymbol{D}_1^{-1}\boldsymbol{D}_2^{-1}\boldsymbol{D}_2 \\ &= \boldsymbol{U}\boldsymbol{L}_2\underline{\boldsymbol{L}}_1^{-1}\boldsymbol{D}_2^{-1}\boldsymbol{D}_1^{-1}\boldsymbol{D}_2 \\ &= \boldsymbol{U}\boldsymbol{L}_2\underline{\boldsymbol{L}}_1^{-1}\boldsymbol{D}_2^{-1}\boldsymbol{D}_1^{-1}\boldsymbol{D}_2 \\ &= \boldsymbol{U}\bar{\boldsymbol{L}}\boldsymbol{D}_1^{-1}\boldsymbol{D}_2. \end{aligned} \tag{A21}$$

Finally, we verify that through proper column scaling, $\boldsymbol{G}$ can become positive definite, and thus reach the result desired. We define a new diagonal matrix

$$\boldsymbol{D}_3 = \begin{bmatrix} \prod_{i=1}^{m} \omega_i & 0 & \cdots & 0 & 0 \\ 0 & \prod_{i=2}^{m} \omega_i & \cdots & 0 & 0 \\ \vdots & \vdots & \ddots & \vdots & \vdots \\ 0 & 0 & \cdots & \omega_m & \\ 0 & 0 & \cdots & 0 & 1 \end{bmatrix}, \tag{A22}$$

then using (A21), we get another key expression

$$\boldsymbol{G}\boldsymbol{D}_1\boldsymbol{D}_2^{-1}\boldsymbol{D}_3^{-1} = \boldsymbol{G}\boldsymbol{D}_2^{-1}\boldsymbol{D}_1\boldsymbol{D}_3^{-1} = \boldsymbol{U}\overline{\boldsymbol{L}}\boldsymbol{D}_3^{-1} = \boldsymbol{U}\boldsymbol{D}_3\boldsymbol{U}^T, \tag{A23}$$

where the last equality follows from $\underline{\boldsymbol{L}}_1^{-1}\boldsymbol{D}_2^{-1} = \boldsymbol{U}^T$ by (A20) and (A22). Hence it follows from Cholesky decomposition that $\boldsymbol{G}\boldsymbol{D}_1\boldsymbol{D}_2^{-1}\boldsymbol{D}_3^{-1} \succ 0$ since $\boldsymbol{D}_3$ is positive and $\boldsymbol{U}$ has all its diagonal entries equal to 1. Let $\boldsymbol{D} = \boldsymbol{D}_1\boldsymbol{D}_2^{-1}\boldsymbol{D}_3^{-1}$, which is a positive diagonal matrix, so it is positive definite, and by (A23) we know $-\boldsymbol{G}\boldsymbol{D}$ is symmetric and negative definite, so

$$-\boldsymbol{G}\boldsymbol{D} - \boldsymbol{D}\boldsymbol{G}^{\boldsymbol{T}} = -2\boldsymbol{G}\boldsymbol{D} \prec 0.$$

Therefore by the Lyapunov matrix equation [31], we deduce that $-\boldsymbol{G}^T$ is Hurwitz, so are $-\boldsymbol{G}$ and $\boldsymbol{F}$. ■

REFERENCES

[1] H. Admiraal and A. Cornaro, "Why underground space should be included in urban planning policy—And how this will enhance an urban underground future," *Tunn. and Und. Space Tech.*, vol. 55, pp. 214–210, May 2016.

[2] W. Broere, "Urban underground space: Solving the problems of today's cities," *Tunn. and Und. Space Tech.*, vol. 55, pp. 245–248, May 2016.

[3] *Urban –Road Tunnels—Recommendations to Managers and Operating Bodies for Design, Management, Operation and Maintenance*, Tech. Comm. On Road Tunn. Oper., PIARC, Paris, France, 2008.

[4] Z. Tan, "Study on inertia effect and linkage control of urban tunnel ventilation," M.S. thesis, Zhejiang Univ., Hangzhou, China, 2013.

[5] T. Du, D. Yang, S. Peng, et al., "A method for design of smoke control of urban traffic link tunnel (UTLT) using longitudinal ventilation," *Tunn. and Und. Space Tech.*, vol. 48, pp. 35–42, Apr. 2015.

[6] Y. Chen, "Discussion of calculation method for multiple-ramp ventilation systems in urban highway tunnels," *Modern Tunn. Tech.*, vol. 48, no. 5, pp. 97–100, May 2011.

[7] C. A. Boman, A. Bring, and T. G. Malmstrom, "Simulation and measurement of road tunnel ventilation," *Tunn. and Under. Space Tech.*, vol. 12, no. 3, pp. 417–424, Jul. 1997.

[8] Z. Tan and H. Gao, "Optimizing vents layout and configuration of complex urban tunnels for air quality control," *IEEE Trans. Control Sys. Tech.* vol. 26, no. 1, pp. 368-376, Jan. 2018.

[9] M. D. Bassett, D. E. Winterbone, and R. J. Pearson, "Calculation of steady flow pressure loss coefficients for pipe junctions," *Proc. of the Inst. of Mech. Eng., Part C, Jour. of Mech. Eng. Sci.*, vol. 215, no. 8, pp. 861–881, Aug. 2001.

[10] W. Chow and M. Chan, "Field measurement on transient carbon monoxide levels in vehicular tunnels," *Build. and Envir.*, vol. 38, no. 2, pp. 227–236, Feb. 2003.

[11] H. Jang and F. Chen, "On the determination of the aerodynamic coefficients of highway tunnels," *Jour. Wind Eng. and Ind. Aerod.*, vol. 90, no. 8, pp. 869–896, Aug. 2002.

[12] M. Sambolek, "Model testing of road tunnel ventilation in normal traffic conditions," *Eng. Struc.*, vol. 26, no. 12, pp. 1705–1711, Oct. 2004.

[13] L. Ferkl and G. Meinsma, "Finding optimal ventilation control for highway tunnels," *Tunn. and Und. Spaces Tech.*, vol. 22, no. 2, pp. 222–229, Mar. 2007.

[14] L. Ferkl, M. Gjerrit, and Š. Michael, "A linear programming approach for ventilation control in tunnels," in *Proc. of the 45th IEEE Conf. on Dec.& Control*, San Diego, CA, USA, pp. 6672–6677, Dec. 2006.

[15] H. Jang and F. Chen, "A novel approach to the transient ventilation of road tunnels," *Jour. Wind Eng. and Ind. Aerod.*, vol. 86, no. 1, pp. 15–36, May 2000.

[16] J. Ling, H. Hao, J. Li, J. Xing, and X. Zheng, "Numerical simulation of natural ventilation in city road tunnel with upper vents," in *Proc. of 2011 Inter. Conf. on Elect. Tech. and Civil Eng.*, Apr. 2011, pp. 5227–5230, Apr. 2011.

[17] Z. Tan, Z. Huang, K. Wu, et al., "Theoretical analysis of longitudinal ventilation system in a road tunnel for predictive control based on inertia effect," *Adv. Mat. Res.*, vol. 639-640, no. 1: pp. 665–669, Jan. 2013.

[18] G. Cheng, M. Qi, J. Zhang, et al., "Analysis of the stability of the ventilation system in Baishan coalmine," *Proc. Eng.*, vol. 45: pp. 311–316, Aug. 2012.

[19] W. Luo, X. Xie, H. Xiao, et al., "Reliability calculation of mine ventilation network," *Proc. Eng.*, vol. 84: pp. 752–757 Jul. 2014.

[20] *Specifications for Design of Ventilation and Lighting of Highway Tunnel.* Chongqing Highway Traffic. Sci. Res. Ins., Minis. of Trans., China, 2000.

[21] Z. Tan and H. O. Gao, "Traffic control for air quality management and congestion mitigation in complex urban vehicular tunnels," *Transp. Res. C, Emerg. Technol.*, vol. 58, pp. 13–28, Sep. 2015.

[22] J. F. Bingham and G. P. Blair, "An improved branched pipe model for multi-cylinder automotive engine calculations," *Proc. of the Inst. of Mech. Eng., Part D, Jour. of Aut. Eng.*, 1985, vol. 199, no. D1, pp. 65–77, Jan. 1985.

[23] V. M. Klell, T. Sams, and A. Wimmer, "Berechnung der Strömung in Rohrverzweigungen," *Motortechnische*, pp. 844–851, Dec.1998.

[24] K. Dvijotham, "System of quadratic equations: Efficient solution algorithms and conditions for solvability," in *Proc. of 53rd Ann. Allerton Conf.*, Allerton, IL, USA, pp. 1027–1031, Sep. 2015.

[25] A. Martegani, G. Pavesi, and C. Barbetta, "The influence of separation, inclination and swirl on single and coupled jet fans installation efficiency," in *Proc. of the 9th Int. Sym. on Aero. and Vent. of Veh. Tun.*, pp. 43–55. Oct. 1997.

[26] Z. Tan, Y. Xia, Q. Yang, et al., "Adaptive fine pollutant discharge control for motor vehicles tunnels under traffic state transition," *IET Intel. Trans. Sys.*, vol. 9, no. 8, pp. 783–791, Jan. 2015.

[27] M. EL-Fadel and Z. Hashisho, "Vehicular emissions and air quality assessment in roadway tunnels: the Salim Slam tunnel," *Trans. Res. Part D*, vol. 5, no. 5, pp. 355-372, May 2000.

[28] S. Azuma, J. Imura, and T. Sugie, "Lebesgue piecewise affine approximation of nonlinear systems," *Nonlin. Anal., Hybrid Syst.*, vol. 4, no. 1, pp. 92–102, Feb. 2010.

[29] R. Fletcher, *Practical Methods of Optimization, Volume 1: Unconstrained Optimization*. Chichester, U.K.: Wiley, 1980.

[30] L.B. Rall, "On the uniqueness of solutions of quadratic equations," *SIAM Review*, vol. 11, no. 3, pp. 386–388, Jul. 1969.

[31] H.K. Khalil, *Nonlinear Systems (3rd edition)*. Prentice-Hall, Upper Saddle River, 2002.